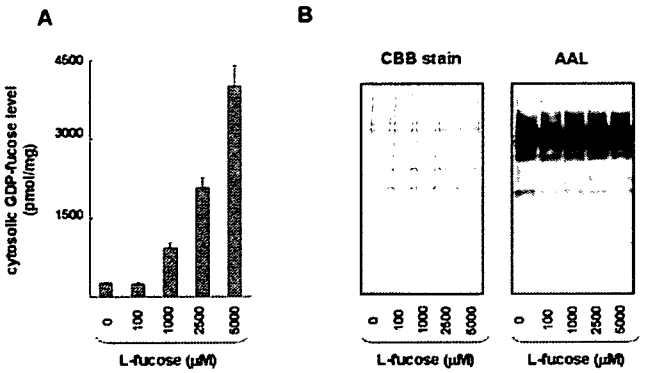

Fig. 5. Cytosolic GDP-fucose and fucosylation in the presence of exogenous L-fucose in Hep3B. (**A**) Cytosolic GDP-fucose level in the presence of L-fucose on represented concentrations was measured as described in "Materials and methods." The results are represented as the means of three independent experiments (*bars*), SD. (**B**) No changes of cellular fucosylation levels in the presence of exogenous L-fucose were observed by AAL lectin blot analysis.

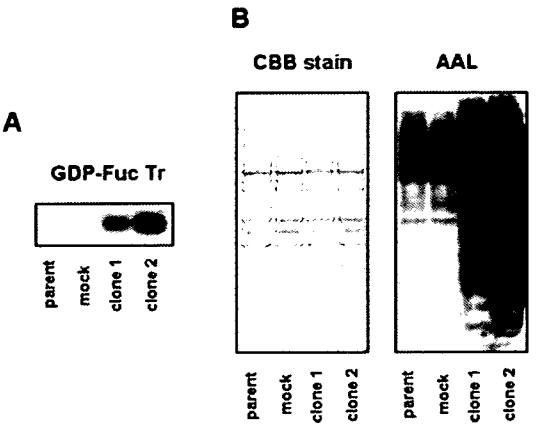

Fig. 6. Analysis of fucosylation level in GDP-Fuc Tr transfectants. (**A**) Total cellular proteins were extracted from parent, mock, and GDP-Fuc Tr transfectants and then a western blot analysis of GDP-Fuc Tr was performed using an anti-V5 antibody. No detection was observed in parent and mock cells because mammalian cells do not contain this epitope. (**B**) AAL lectin blot analysis was performed using total cellular proteins.

Effect of the addition of exogenous L-*fucose on hepatoma cell line, Hep3B*

To demonstrate the direct involvement of GDP-fucose in the regulation of fucosylation in hepatoma cells, various concentrations of L-fucose were added to the condition medium of Hep3B cells. L-Fucose was incorporated into the cells and converted to GDP-fucose via the salvage pathway (Smith et al. 2002; Luhn et al. 2004). After culturing for 72 h in the presence of L-fucose, cytosolic GDP-fucose was increased in proportion to the concentration of L-fucose in the condition medium and was increased by about 16-fold in the presence of 5000 μM L-fucose (Figure 5A). In the case of the presence of 100 μM L-fucose, no elevation in cytosolic GDP-fucose was detected. We subsequently analyzed the change in fucosylation level by means of an AAL lectin blot. As shown in Figure 5B, cellular fucosylation was not increased at all. When we cultured the cells in the presence of 5000 μM L-fucose for 4 weeks, we observed no increase in fucosylation (data not shown). Accordingly, even when cytosolic GDP-fucose was extremely increased, cellular fucosylation was not changed, suggesting that GDP-fucose levels are not a rate-limiting factor for the total cellular fucosylation in Hep3B cells.

The effect of overexpression of GDP-fucose transporter on fucosylation level

To determine whether or not GDP-Fuc Tr is directly involved in regulating fucosylation in HCC, we investigated the effects of the GDP-Fuc Tr gene transfection on the level of fucosylation in Hep3B cells. Two transfectants of GDP-Fuc Tr were established through selection by G418 treatment (clone 1 and 2). Western blot analysis using anti-V5 antibody, which recognized a tag sequence in GDP-Fuc Tr expression vector, showed a high expression of GDP-Fuc Tr in the transfectants (Figure 6A). To investigate changes in the fucosylation levels, we performed a lectin blot analysis using AAL lectin. As shown in Figure 6B, fucosylation levels were dramatically increased in the transfectants. Clone 2, which expressed higher level of GDP-Fuc Tr than clone 1, showed a much higher increase in fucosylation. To deny secondary effects of overexpression of GDP-Fuc Tr on other fucosylation-related genes, expressions of FX and GMD were investigated by real-time RT-PCR analysis. As expected, expression of FX and GMD mRNA was not changed among transfectants of GDP-Fuc Tr, parent and mock (Supplementary data, Figure 2). These results show that GDP-Fuc Tr is able to efficiently upregulate the influx of GDP-fucose from the cytosol to the Golgi lumen followed by increases in the cellular fucosylation. Rather than cytosolic GDP-fucose, it is GDP-Fuc Tr that is mainly involved in the regulation of cellular fucosylation in Hep3B cells.

Correlation between the expression of GDP-fucose transporter and the cellular fucosylation in HCC tissues

The expression level of GDP-Fuc Tr and how it relates to cellular fucosylation in vivo were investigated using tissue microarray (Figure 7A, B, and C). This microarray includes 59 HCCs of various stages. The HCC serial sections that showed positive stainings for AAL, GDP-Fuc Tr, and α1-6 FucT are shown in Figure 7D, E, and F. In contrast, the sections that showed positive stainings for AAL and GDP-Fuc Tr, but negative for α1-6 FucT are shown in Figure 7 G, H and I, indicating that the expression of GDP-Fuc Tr resulted in the increases of fucosylation even below the detectable level of α1-6 FucT. The positive stainings of GDP-Fuc Tr and α1-6 FucT were observed as a Golgi-localized pattern. Of the 59 cases, 38 cases showed AAL (+) and GDP-Fuc Tr (+), and 8 cases showed AAL (−) and GDP-Fuc Tr (−), indicating that the expression of GDP-Fuc Tr was highly correlated with the cellular fucosylation in vivo (Table IA). There was no correlation between α1-6 FucT and AAL stainings (Table IB). These results indicate that GDP-Fuc Tr directly regulates the cellular fucosylation in vivo and is the most important factor for the increases of fucosylation in HCC.

Discussion

Alterations in the expression of fucosylated oligosaccharides are observed in a variety of biological and pathological

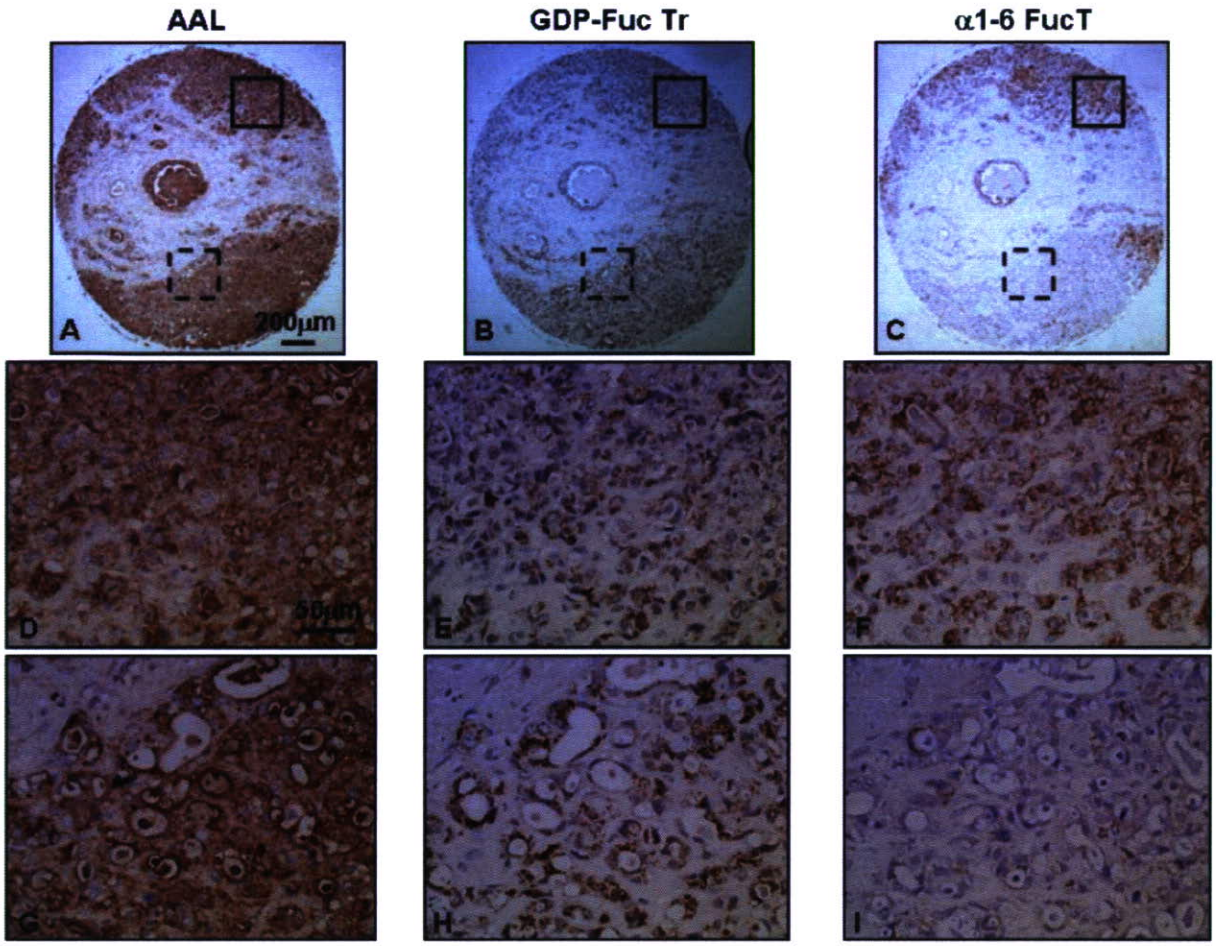

Fig. 7. Immunohistochemical staining patterns for AAL, GDP-Fuc Tr, and α1-6 FucT in HCC. The serial sections of HCC were stained using tissue microarray by AAL, anti-GDP-Fuc Tr, and anti-α1-6 FucT antibody (**A**, **B**, and **C**) as described in "Materials and methods". The area in the square and the dotted square was magnified in the medial (**D**, **E**, and **F**) and the lower column (**G**, **H**, and **I**), respectively.

Table I. Correlation between expression level of (A) GDP-Fuc Tr and cellular fucosylation; (B) α1-6 FucT and cellular fucosylation

		(A) GDP-Fuc Tr[a]				(B) α1-6 FucT[b]		
		+	−	Total		+	−	Total
AAL	+	38	4	42	+	20	22	42
	−	9	8	17	−	12	5	17
	Total	47	12	59	Total	32	27	59

[a] $P < 0.01$, compared between expression level of GDP-Fuc Tr and intensity of AAL staining (Fisher's test).
[b] Not significant, compared between expression level of α1-6 FucT and intensity of AAL staining (Fisher's test).

conditions. Above all, fucosylated oligosaccharides have clearly been related to malignant tumors in numerous studies conducted over the past several decades (Tatsumura et al. 1977). Therefore, an advanced understanding of the underlying mechanism of fucosylation would provide new strategies for the treatment and diagnosis for malignant tumors.

We previously reported that the expression level of FX was increased in HCC compared with chronic liver disease and normal liver, but that α1-6 FucT was not increased compared with chronic liver disease (Noda et al. 1998; Noda et al. 2003). However, which factors in fucosylation-related genes are responsible for the increases of fucosylation in HCC remains unknown. In the present study, the expression levels of fucosylation-related genes, such as FX and α1-6 FucT, GDP-Fuc Tr, GMD, and GDP-fucose pyrophosphorylase, were comprehensively investigated by real-time RT-PCR analyses. It was found that GDP-Fuc Tr is also significantly increased in HCC compared with chronic liver disease and normal liver. In a recent study by another group, the expression levels of FX, GMD, and GDP-Fuc Tr mRNA were reportedly increased in acute inflammation using a rat kidney allograft for a model system, but GDP-fucose pyrophosphorylase was not increased (Niittymaki et al. 2006). In the present study using human liver tissue, similar changes were observed during chronic inflammation. As shown in Figure 2B, the expressions of FX, GMD, and GDP-Fuc Tr were increased in chronic liver disease compared with normal livers, but the expression of GDP-fucose pyrophosphorylase was not increased. These results suggest that fucosylation-related genes such as GDP-Fuc Tr, FX, and GMD are involved in certain types of inflammation. However, the levels of GDP-Fuc Tr, FX, and GMD

were much more increased in HCC tissues, indicating that these fucosylation-related factors are involved in carcinogenesis.

The increased expression of the GMD protein, which is independent of the upregulation of GMD mRNA, suggests the unknown posttranslational regulation of GMD in HCC (Figure 3). Nakayama et al. reported that in *Arabidopsis thaliana*, AtFX/GER1 (*A. thaliana* homolog of human FX) contributed to the maintenance of MUR1 (*A. thaliana* homolog of human GMD) as the active form by forming a complex, resulting in the stabilization of MUR1 activity (Nakayama et al. 2003). In the case of human HCC, an increased expression of FX might increase the stabilization of GMD, resulting in increases in GDP-fucose levels. Further analyses of interactions between human FX and GMD could shed new light on our understanding of the regulatory mechanisms of fucosylation in HCC.

To know which factors are important for the increases of fucosylation in HCC, expression levels of GDP-Fuc Tr, FX, and GMD were compared with total cellular fucosylation in hepatoma cells. As shown in Figure 4, both HepG2 and Huh7 cells with high expression levels of GDP-Fuc Tr, FX, and GMD showed high fucosylation levels. In contrast, Hep3B cells showed a low fucosylation level in spite of the relatively high expression levels of FX and GMD because of the low expression level of GDP-Fuc Tr. Even when the expression levels of FX and GMD were high, cellular fucosylation did not increase appreciably, indicating that GDP-Fuc Tr could be a rate-limiting factor for fucosylation.

The extreme elevation of cytosolic GDP-fucose by the addition of a large excess of L-fucose in Hep3B cells resulted in no elevation in cellular fucosylation. On the other hand, the elevation of GDP-Fuc Tr could directly lead to a drastic elevation in fucosylation, which would mean, therefore, that GDP-Fuc Tr could effectively upregulate cellular fucosylation in Hep3B cells. These results indicate that cytosolic GDP-fucose has been already in abundance and available for the transport by GDP-Fuc Tr even before the addition of exogenous L-fucose. In a previous study, the overexpression of FX in Hep3B cells resulted in a slight elevation in cellular fucosylation (Noda et al. 2003). Overexpression of FX leads to the increase in cytosolic GDP-fucose via de novo pathway. However, even if cytosolic GDP-fucose is increased, cellular fucosylation does not change without enhancement of GDP-Fuc Tr expression (Figure 5). Therefore, the increase of fucosylation by overexpression of FX in our previous study might be due to an indirect effect of increases in FX expression, which is independent of GDP-fucose synthesis. Functional interaction among FX, GMD, and GDP-Fuc Tr should be investigated in further studies.

To investigate the more direct relationship between the expression of fucosylation-related genes and cellular fucosylation in many HCC tissues, an immunohistochemical study was performed. Positive stainings of AAL and GDP-Fuc Tr were observed in 42/59 cases and 47/59 cases, respectively, and their expression was highly correlated. In contrast, 12/32 cases of α1-6 FucT positive tissues showed negative/low staining for AAL, suggesting that GDP-fucose Tr, but not α1-6 FucT, regulates cellular fucosylation in HCC tissues. When AOL lectin, which recognizes α1-6 linked fucose more specifically (Matsumura et al. 2007), was used for this immunohistochemical study, a positive signal was weak due to the quality of tissue microarray and the data was almost the same with that of AAL (data not shown).

This study demonstrated the importance of the upregulation of GDP-Fuc Tr in cellular fucosylation using human HCC tissues and hepatoma cell lines. Since fucosylation could regulate the malignant potential of cancer cells, we conclude that GDP-Fuc Tr could serve as a new target for the advanced treatment and diagnosis of HCC.

Materials and methods

Patients and liver tissue specimens

Surgical specimens were obtained from 13 HCC patients, aged 63 ± 3.4 years (9 males and 4 females), during surgical operations and were processed as described previously (Noda et al. 1998). Of these patients, 7, 5, and 1 exhibited CH, LC, and normal liver in the adjacent tissue of HCC, respectively. In addition, 2 patients, aged 58.5, with liver metastasis of colon cancer who were serologically and histologically negative for any chronic liver disease were used as controls (1 male and 1 female). This research was approved by the ethical committee of the hospital. Tumor samples and adjacent liver tissues were obtained and stored in liquid nitrogen until used.

RNA extraction and real-time RT-PCR

RNA was extracted from frozen specimens of 13 patients, two normal livers and five hepatoma cells – Hep3B, HepG2, HLE, HLF, and Huh7 – with the TRIsol reagent, according to the manufacturer's instructions (Invitrogen, Carlsbad, CA). The concentrations of all RNA samples were determined spectrophotometrically and stored at −80°C until used. RNA contained 1× M-MLV buffer, 0.5 mM dNTP mixture, 50 pmol Random 6 mers, 50 U M-MLV RTase and 10 U RNase inhibitor was adjusted to a volume of 10 μL with RNase-free distilled H_2O and reverse-transcripted for 15 min at 42°C and 2 min at 95°C (TAKARA BIO, Siga, Japan). Each PCR product was then adjusted to a volume of a 25 μL solution containing 1×SYBR Premix Ex Taq, 0.2 μM forward and reverse primers. Real-time PCR analysis was carried out using the Smart Cycler System (TAKARA BIO). Primers for GDP-Fuc Tr, FX, GMD, GDP-fucose pyrophosphorylase, α1-6 FucT, hypoxanthine guanine phosphoribosyl transferase (HPRT), and glyceraldehyde-3-phosphate dehydrogenase (GAPDH) genes used in this study are summarized in Table II. Both HPRT and GAPDH were used as an internal control. The results were normalized as relative values using HPRT for clinical samples and GAPDH for hepatoma cell lines as a reference to compare the mRNA expression.

Antibody

Anti-GMD and anti-GDP-Fuc Tr polyclonal antibody was developed by immunization of the bovine thyroglobulin-conjugated C-terminated peptide of GMD and GDP-Fuc Tr into a rabbit followed by purification by protein G, respectively (Immuno-Biological Laboratories Co., Ltd., Gunma, Japan). Mouse anti-V5, which is 14 amino acids epitope derived from the P and V proteins of the paramyxovirus, SV5, and anti-α1-6 FucT monoclonal antibody was obtained from Invitrogen and Fujirebio Inc. (Tokyo, Japan), respectively.

Western blot analysis

The cells were harvested from a 10 cm dish. After precipitation by centrifugation at 2000 rpm for 5 min at 4°C, they were

Table II. Primer sequences for the genes examined in the present study

mRNA	Sequence	Size of primer (bp)
GDP-Fuc Tr	F : 5′-TGCTCACCTGCGGTATCATCA-3′	21
	R : 5′-TCTGGCTTGGTGTGGACCAG-3′	20
FX	F : 5′-GGTAGCAGATGGAGCTGGACTT-3′	22
	R : 5′-GAAGGTCCAACCCACACACGT-3′	21
GMD	F : 5′-ATTGTACGGCGGTCCAGTTCA-3′	21
	R : 5′-GAAGTTGCACTATGGCGATCTCACT-3′	25
GDP-fucose	F : 5′-GCAATAACAGCGGCTGATGAA-3′	21
pyrophosphorylase	R : 5′-AAGGGCACAAAGTGTTGATCCTC-3′	23
α1-6 FucT	F : 5′-CAGCGAACACTCATCTTGGAA-3′	21
	R : 5′-GACATGCACAGACAGATCTGGC-3′	22
HPRT	F : 5′-TGACACTGGCAAAACAATGCA-3′	21
	R : 5′-GGTCCTTTTCACCAGCAAGCT-3′	21
GAPDH	F : 5′-ATTGCCCTCAACGACCACTT -3′	20
	R : 5′-AGGTCCACCACCCTGTTGCT -3′	20

F: Forward primer.
R: Reverse primer.

resuspended in TNE buffer (10 mM Tris-HCl [pH 7.8], 1% NP40, 0.15 M NaCl, 1 mM ethylenediaminetetraacetic acid [EDTA]) including a protease inhibitor cocktail (Roche, Basel, Switzerland), and then placed on ice for 30 min to allow solubilization. These samples were then centrifuged at 15,000 rpm for 15 min at 4°C and the supernatants were collected. These cell lysates were quantitated using a Bicinchoninic Acid kit (BCA kit, Pierce, Rockford, IL). Cell lysates were subjected to sodium dodecyl sulfate-polyacrylamide gel electrophoresis (SDS-PAGE) under reducing conditions and then transferred to a polyvinylidine difluoride (PVDF) membrane (Millipore, Woburn, MA). After blocking with phosphate-buffered saline (PBS) containing 5% skim milk for 1 h at room temperature (RT), the membrane was incubated with rabbit anti-GMD polyclonal antibody or mouse anti-V5, which is 14 amino acids epitope derived from the P and V proteins of the paramyxovirus, SV5, monoclonal antibody for 1 h at RT. After washing the membrane twice with Tris-buffered saline, containing 0.05% Tween 20 (TBST) (pH 7.4), it was incubated with diluted horseradish peroxidase-conjugated anti-rabbit IgG (Cell Signaling, Beverly, MA) or anti-mouse IgG (Promega, Madison, WI) for 1 h at RT. It was again washed two times and developed with an enhanced chemiluminescence system (ECL kit, GE Healthcare BioSciences, the Chalfont St. Giles, United Kingdom) according to the manufacturer's protocol. Immunoreactivity was quantified by scanning densitometry.

Measurement of cytosolic GDP-fucose concentration

Measurement of the cytosolic GDP-fucose concentration was performed as described previously with minor modifications (Noda et al. 2002). Cells harvested from a 10 cm dish were precipitated by centrifugation at 2000 rpm for 5 min at 4°C and resuspended in a 0.25 M sucrose buffer supplemented with 10 mM Tris-HCl (pH 7.4), 10 mM KCl, 10 mM $MgCl_2$, 5 mM adenosine-5-monophosphate (AMP) (pH 7.4) (Wako, Osaka, Japan) and a protease inhibitor cocktail. The cells were homogenized with a Dounce homogenizer and then centrifuged at 500 × *g* for 5 min at 4°C to remove cell debris and nuclei. The supernatants were then subjected to ultracentrifugation (Optima TL Ultracentrifuge, TLA-45 rotor, Beckman, Fullerton, CA) at 40,000 rpm for 1 h at 4°C to give the cytosolic fraction. The supernatants were quantitated using a BCA kit.

The above proteins were adjusted to a volume of 20 μL with cold H_2O. After the addition of 8 μL of 1 M MES-NaOH (pH 7.0), the samples were boiled at 100°C for 20 s to inactivate endogenous enzymes that use or degrade GDP-fucose. The samples were then centrifuged at 15,000 rpm for 15 min at 4°C. The samples were mixed with 1 μL of 10% Triton X-100, 2 μL of 100 μM fluorescent-labeled acceptor substrate and 4 μL of purified recombinant α1-6 FucT. The mixtures were incubated at 37°C for 2 h to allow the contained GDP-fucose to attach to the acceptor substrate by the action of α1-6 FucT. The reactions were terminated by boiling at 100°C for 3 min. The samples were centrifuged at 15,000 rpm for 15 min. Then, 30 μL of the 35 μL supernatants were subjected to HPLC (Shimadzu, Kyoto, Japan). Finally, the areas of fluorescent intensity of fucosylated acceptor substrates were converted to GDP-fucose concentrations using a standard curve of 0–50 pmol GDP-fucose.

Lectin blot analysis

Duplicate samples were subjected to SDS-PAGE under reducing conditions. One gel was subjected to Coomassie Brilliant Blue R-250 staining and the other was transferred to a PVDF membrane for AAL lectin blot analysis. AAL interacts with fucosylated oligosaccharides (Yamashita et al. 1985). After blocking with PBS containing 3% BSA overnight at 4°C, the membrane was incubated in diluted biotinylated AAL (Seikagaku Corp., Tokyo, Japan) for 40 min at RT. It was then washed three times with TBST and incubated with diluted avidin-peroxidase conjugates (ABC kit, Vector Res. Corp., Burlingame, CA) for 40 min at RT. The membrane was again washed three times with TBST and developed with an ECL system.

Cells culture and transfection

Human hepatoma cell lines, Hep3B, HepG2, HLE, HLF, and Huh7, provided from the ATCC (American Type Culture Collection, Manassas, VA) were cultured in RPMI1640 supplemented with 100 U/mL penicillin, 100 μg/mL streptomycin and 10% FCS.

Human GDP-Fuc Tr cDNA was prepared by PCR using a human spleen cDNA library (TAKARA BIO) as a template and the following forward and reverse primers were designed: 5′-ACCATGAATAGGGCCCCTCTG-3′ and 5′-CACCCCCATGGCGCTCTTCTC-3′, respectively. The obtained DNA fragment was inserted into a pcDNA3.1/V5-His TOPO vector (Invitorogen), which is regulated by the cytomegalovirus (CMV) promoter and has the V5 epitope at the C-terminal. Vector insertion was confirmed by sequencing. This construct was transfected to Hep3B cells by the modified polycationic transfection method using the Effectene Transfection Reagent (Qiagen, Hilden, Germany) according to the manufacturer's protocol. Selection was performed by the addition of 700 μg/mL geneticin (G418 disulfate) (nacalai tesque, Kyoto, Japan).

Immunohistochemical analysis

We used the tissue microarray including 59 liver carcinomas (KURABO, Osaka, Japan). In brief, tissue microarray slides were deparaffinized with xylene and ethanol. Antigen retrieval was performed using citrate buffer (pH 6.0). Then, they were pretreated with Peroxidase Blocking Reagent (DAKO,

Carpinteria, CA) for 10 min at RT. After washing twice with PBS, they were incubated with TBST containing 5% BSA overnight at 4°C for AAL staining or Protein Block Serum-Free (DAKO) for 30 min at RT for the others. They were incubated with biotinylated AAL (2.0 μg/mL) for 1 h at RT or anti-GDP-Fuc Tr and anti-α1-6 FucT antibodies overnight at 4°C. They were then washed three times with PBS and incubated with ABC kit for 30 min at RT for AAL staining or EnVision System Labelled Polymer-HRP Anti-rabbit and mouse (DAKO) for 30 min at RT for GDP-Fuc Tr staining and α1-6 FucT staining, respectively. After washing three times with PBS, positive staining was visualized using diaminobenzidine (DAKO) and counterstaining was performed with hematoxylin. Slides were also stained in the absence of primary antibody to evaluate non-specific secondary antibody reactions.

Statistical analyses

The results are represented as the mean ± SD. In comparing variables in more than two groups, a one-way ANOVA analysis was performed, followed by a Fisher's PLSD test if the former was significant. Fisher's test was adopted in the immunohistochemical analyses. Results of $P < 0.05$ were considered to be significant.

Supplementary data

Supplementary data for this article is available online at www.glycob.oxfordjournals.org

Funding

Japan Science and Technology Agency (JST); 21st Century Center of Excellence program from the Ministry of Education, Culture, Sports, Science, and Technology of Japan; New energy and Industrial Technology Development Organization; Health and Labour Sciences Research Grants from Ministry of Health, Labour and Welfare.

Acknowledgements

We thank Dr. Hideyuki Ihara (Department of Disease Glycomics, Research Institute for Microbial Diseases, Osaka University) and Dr. Yoko Mizuno-Horikawa (Department of Biochemistry, Osaka University Graduate School of Medicine) for providing a fluorescent-labeled acceptor substrate for the measurement of cytosolic GDP-fucose concentration and technical advice for immunohistochemical analyses, respectively.

Conflict of interest statement

None declared.

Abbreviations

AAL, *Aleuria aurantia lectin*; AFP, alpha-fetoprotein; α1-6 fucosyltransferase, GDP-L-Fuc : *N*-acetyl-β-D-glucosaminide α1-6 fucosyltransferase; CH, chronic hepatitis; CL, liver cirrhosis; FX, GDP-4-keto-6-deoxy-mannose-3, 5-epimerase-4-reductase; GDP, guanosine 5′-diphosphate; GDP-Fuc Tr, GDP-fucose transporter; GADPH, glyceraldehyde-3-phosphate dehydrogenase; GMD, GDP-mannose 4, 6-dehydratase; GMP, guanosine 5′-monophosphate; HCC, hepatocellular carcinoma; HPLC, high performance liquid chromatography; HPRT, hypoxanthine guanine phosphoribosyl transferase; LEC rat, Long-Evans with cinnamon-like coat color rat; PBS, phosphate-buffered saline; PLSD, protected least significant differences; PVDF, polyvinylidine difluoride; RT-PCR, reverse transcription polymerase chain reaction; SDS-PAGE, sodium dodecyl sulfate-polyacrylamide gel electrophoresis.

References

Alpert ME, Uriel J, and de Nechaud B 1968. Alpha-1 fetoglobulin in the diagnosis of human hepatoma. N Engl J Med. 278:984–986.

Aoyagi Y, Isemura M, Yosizawa Z, Suzuki Y, Sekine C, Ono T, and Ichida F 1985. Fucosylation of serum alpha-fetoprotein in patients with primary hepatocellular carcinoma. Biochim Biophys Acta. 830:217–223.

Chen DS and Sung JL 1977. Serum alphafetoprotein in hepatocellular carcinoma. Cancer.40:779–783.

Ebara M, Ohto M, Shinagawa T, Sugiura N, Kimura K, Matsutani S, Morita M, Saisho H, Tsuchiya Y, and Okuda K 1986. Natural history of minute hepatocellular carcinoma smaller than three centimeters complicating cirrhosis. A study in 22 patients. Gastroenterology. 90:289–298.

Hakomori S 1989. Aberrant glycosylation in tumors and tumor-associated carbohydrate antigens. Adv Cancer Res. 52:257–331.

Hirschberg CB 2001. Golgi nucleotide sugar transport and leukocyte adhesion deficiency II. J Clin Invest. 108:3–6.

Kumamoto K, Goto Y, Sekikawa K, Takenoshita S, Ishida N, Kawakita M, and Kannagi R 2001. Increased expression of UDP-galactose transporter messenger RNA in human colon cancer tissues and its implication in synthesis of Thomsen-Friedenreich antigen and sialyl Lewis A/X determinants. Cancer Res. 61:4620–4627.

Luhn K, Laskowska A, Pielage J, Klambt C, Ipe U, Vestweber D, and Wild MK 2004. Identification and molecular cloning of a functional GDP-fucose transporter in Drosophila melanogaster. Exp Cell Res, 301:242–250.

Matsumura K, Higashida K, Ishida H, Hata Y, Yamamoto K, Shigeta M, Mizuno-Horikawa Y, Wang X, Miyoshi E, Gu J, and Taniguchi N 2007. Carbohydrate-binding specificity of a fucose-specific lectin from aspergillus oryzae: A novel probe for core fucose. J Biol Chem. 282:15700–15708.

Nakayama K, Maeda Y, and Jigami Y 2003. Interaction of GDP-4-keto-6-deoxymannose-3,5-epimerase-4-reductase with GDP-mannose-4,6-dehydratase stabilizes the enzyme activity for formation of GDP-fucose from GDP-mannose. Glycobiology, 13:673–680.

Niittymaki J, Mattila P, and Renkonen R 2006. Differential gene expression of GDP-L-fucose-synthesizing enzymes, GDP-fucose transporter and fucosyltransferase VII. Apmis. 114:539–548.

Noda K, Miyoshi E, Gu J, Gao CX, Nakahara S, Kitada T, Honke K, Suzuki K, Yoshihara H, Yoshikawa K, Kawano K, Tonetti M, Kasahara A, Hori M, Hayashi N, and Taniguchi N 2003. Relationship between elevated FX expression and increased production of GDP-L-fucose, a common donor substrate for fucosylation in human hepatocellular carcinoma and hepatoma cell lines. Cancer Res. 63:6282–6289.

Noda K, Miyoshi E, Nakahara S, Ihara H, Gao CX, Honke K, Yanagidani S, Sasaki Y, Kasahara A, Hori M, Hayashi N, and Taniguchi N 2002. An enzymatic method of analysis for GDP-L-fucose in biological samples, involving high-performance liquid chromatography. Anal Biochem. 310:100–106.

Noda K, Miyoshi E, Uozumi N, Gao CX, Suzuki K, Hayashi N, Hori M, and Taniguchi N 1998. High expression of alpha-1–6 fucosyltransferase during rat hepatocarcinogenesis. Int J Cancer, 75:444–450.

Noda K, Miyoshi E, Uozumi N, Yanagidani S, Ikeda Y, Gao C, Suzuki K, Yoshihara H, Yoshikawa K, Kawano K, Hayashi N, Hori M, and Taniguchi N 1998. Gene expression of alpha1–6 fucosyltransferase in human hepatoma tissues:a possible implication for increased fucosylation of alpha-fetoprotein. Hepatology. 28:944–952.

Nordeen MH, Jones SM, Howell KE, and Caldwell JH. 2000. GOLAC: an endogenous anion channel of the Golgi complex. Biophys J. 78:2918–2928.

Ohyama C, Smith PL, Angata K, Fukuda MN, Lowe JB, and Fukuda M 1998. Molecular cloning and expression of GDP-D-mannose-4,6-dehydratase, a key enzyme for fucose metabolism defective in Lec13 cells. J Biol Chem. 273:14582–14587.

Park SH, Pastuszak I, Drake R, and Elbein AD 1998. Purification to apparent homogeneity and properties of pig kidney L-fucose kinase. J Biol Chem. 273:5685–91.

Pastuszak I, Ketchum C, Hermanson G., Sjoberg EJ, Drake R, and Elbein AD 1998. GDP-L-fucose pyrophosphorylase. Purification, cDNA cloning, and properties of the enzyme. J Biol Chem. 273:30165–30174.

Smith PL, Myers JT, Rogers CE, Zhou L, Petryniak B, Becker DJ, Homeister JW, and Lowe JB 2002. Conditional control of selectin ligand expression and global fucosylation events in mice with a targeted mutation at the FX locus. J Cell Biol. 158:801–815.

Sullivan FX, Kumar R, Kriz R, Stahl M, Xu GY, Rouse J, Chang XJ, Boodhoo A, Potvin B, and Cumming DA 1998. Molecular cloning of human GDP-mannose 4,6-dehydratase and reconstitution of GDP-fucose biosynthesis in vitro. J Biol Chem. 273:8193–8202.

Taketa K, Endo Y, Sekiya C, Tanikawa K, Koji T, Taga H, Satomura S, Matsuura S, Kawai T, and Hirai H 1993. A collaborative study for the evaluation of lectin-reactive alpha-fetoproteins in early detection of hepatocellular carcinoma. Cancer Res. 53:5419–5423.

Tatsumura T, Sato H, Mori A, Komori Y, Yamamoto K, Fukatani G, and Kuno S 1977. Clinical significance of fucose level in glycoprotein fraction of serum in patients with malignant tumors. Cancer Res. 37:4101–4103.

Tonetti M, Sturla L, Bisso A, Benatti U, and De Flora A. 1996. Synthesis of GDP-L-fucose by the human FX protein. J Biol Chem. 271:27274–27279.

Uozumi N, Yanagidani S, Miyoshi E, Ihara Y, Sakuma T, Gao CX, Teshima T, Fujii S, Shiba T, and Taniguchi N 1996. Purification and cDNA cloning of porcine brain GDP-L-Fuc:N-acetyl-beta-D-glucosaminide alpha1–>6fucosyltransferase. J Biol Chem. 271:27810–27817.

Yamashita K, Kochibe N, Ohkura T, Ueda I, and Kobata A 1985. Fractionation of L-fucose-containing oligosaccharides on immobilized Aleuria aurantia lectin. J Biol Chem. 260:4688–4693.

Yanagidani S, Uozumi N, Ihara Y, Miyoshi E, Yamaguchi N, and Taniguchi N 1997. Purification and cDNA cloning of GDP-L-Fuc:N-acetyl-beta-D-glucosaminide:alpha1–6 fucosyltransferase (alpha1–6 FucT) from human gastric cancer MKN45 cells. J Biochem (Tokyo). 121:626–632.

Zipin A, Israeli-Amit M, Meshel T, Sagi-Assif O, Yron I, Lifshitz V, Bacharach E, Smorodinsky NI, Many A, Czernilofsky PA, Morton DL, and Witz IP 2004. Tumor-microenvironment interactions: the fucose-generating FX enzyme controls adhesive properties of colorectal cancer cells. Cancer Res. 64:6571–6578.

Glycobiology vol. 18 no. 1 pp. 114–124, 2008
doi:10.1093/glycob/cwm107
Advance Access publication on October 2, 2007

Reduced α4β1 integrin/VCAM-1 interactions lead to impaired pre-B cell repopulation in alpha 1,6-fucosyltransferase deficient mice

Wenzhe Li[2], Katsuhiko Ishihara[5], Takafumi Yokota[3], Takatoshi Nakagawa[2], Nobuto Koyama[6], Jinhua Jin[4], Yoko Mizuno-Horikawa[7], Xiangchun Wang[4], Eiji Miyoshi[7], Naoyuki Taniguchi[8], and Akihiro Kondo[1,2]

Departments of [2]Glycotherapeutics [3]Hematology and Oncology; and [4]Biochemistry, Osaka University Graduate School of Medicine, Osaka 565-0871, Japan; [5]Department of Immunology and Molecular Genetics, Kawasaki Medical School, Okayama 701-0192, Japan; [6]Takara Bio Inc., Shiga 520-2193, Japan; [7]Department of Functional Diagnostic Science, Division of Health Science, Osaka University School of Health Sciences, Osaka 565-0871, Japan; and [8]Department of Disease Glycomics, Research Institute for Microbial Diseases, Osaka University, Osaka 565-0871, Japan

Received on August 14, 2007; revised on September 21, 2007; accepted on September 27, 2007

Mice with a targeted gene disruption of *Fut8* (*Fut8*$^{-/-}$) showed an abnormality in the transition from pro-B cell to pre-B cell, reduced peripheral B cells, and a decreased immunoglobulin production. Alpha 1,6-fucosyltransferase (FUT8) is responsible for the alpha 1,6 core fucosylation of *N*-glycans, which could modify the functions of glycoproteins. The loss of a core fucose in both very late antigen 4 (VLA-4, α4β1 integrin) and vascular cell adhesion molecule 1 (VCAM-1) led to a decreased binding between pre-B cells and stromal cells, which impaired pre-B cells generation in *Fut8*$^{-/-}$ mice. Moreover, the B lineage genes, such as *CD79a*, *CD79b*, *Ebf1*, and *Tcfe2a*, were downregulated in *Fut8*$^{-/-}$ pre-B cells. Indeed, the frequency of preBCR^{+}CD79b^{low} cells in bone marrow pre-B cells in *Fut8*$^{-/-}$ was much lower than that in *Fut8*$^{+/+}$ cells. These results reveal a new role of core fucosylated *N*-glycans in mediating early B cell development and functions.

Keywords: alpha 1,6-fucosyltransferase/B-cell development/CD45R; *N*-glycans/α4β1 integrin/VCAM-1

Introduction

B lymphocytes differentiate in the bone marrow (BM) from hematopoietic stem cells through a sequential series of intermediates, which are characterized by cell surface antigens and immunoglobulin rearrangement (Hardy and Hayakawa 2001; Pelayo et al. 2005). Precursor B cells develop in close interaction with the BM environment. Adhesion molecules, including CD44, selectin, and integrins, control the interaction between B cell progenitors and BM stromal cells or extracellular matrix (ECM) components. The integrins comprise a large family of heterodimeric transmembrane molecules consisting of α and β subunits, which mediate adhesion, migration, the survival and differentiation of the cells (Hynes 1992). Cell surface integrins are all major carriers of *N*-glycans, and the *N*-glycosylation of integrins plays an important role in their biological functions (Pochec et al. 2003; Gu and Taniguchi 2004).

GDP-L-Fuc:*N*-acetyl-β-D-glucosaminide α1,6-fucosyltransferase (FUT8) catalyzes the transfer of a fucose residue from GDP-fucose to the innermost GlcNAc residue of complex *N*-glycans via an α1,6-linkage (core fucosylation) in the golgi apparatus in mammals (Wilson et al. 1976). *Fut8* deficient (*Fut8*$^{-/-}$) mice showed a postnatal failure to thrive, and all of the survivors manifested growth retardation and emphysema-like changes (Wang et al. 2005). We recently reported that signaling through the transforming growth factor-β (TGF-β) receptor (Wang et al. 2005) and the epidermal growth factor (EGF) receptor (Li et al. 2006) was downregulated in *Fut8*$^{-/-}$ mice, due to a decreased ligand affinity for the receptor. Shinkawa et al. (2003) reported that deletion of the core fucose from Cγ2 of IgG1 enhanced antibody-dependent cell-mediated cytotoxity (ADCC) activity by up to 50–100 fold. Collectively, these results strongly suggest that the core fucosylation of *N*-glycans modifies the function of the corresponding glycoprotein.

Integrins bind to ECM components such as fibronectin and laminin as well as cellular receptors such as vascular adhesion molecule-1 (VCAM-1), thereby facilitating signal transduction from stromal cell-derived soluble factors such as IL-7, which are important for the survival of B cell precursors (Hynes 1992). Very late antigen-4 (VLA-4; CD49d/CD29; α4β1 integrin) belongs to the integrin family of cell adhesion molecules and is expressed by a wide range of leucocytes (Springer 1990). α4β1 integrin is expressed at high levels on the surface of lymphohematopoietic progenitors, and is involved in their development and proliferation (Miyake et al. 1991; Grabovsky et al. 2000). In addition, its interaction with fibronectin and/or VCAM-1 mediates leukocyte tethering, rolling, and firm adhesion on the endothelium, which is indispensable for recruiting leukocytes to inflammatory tissues (Vonderheide et al. 1994; Alon et al. 1995). VCAM-1, a ligand of α4β1 integrin, is constitutively expressed by the BM stromal cells (Miyake et al. 1991) and by the follicular dendritic cells (Koopman et al. 1991). Indeed, pre-B cells fail to transmigrate and proliferate in the absence of α4 integrins (Arroyo et al. 1999), and conditional VCAM-1 mutant mice show an impaired humoral immune response against the T cell dependent antigens (Leuker et al. 2001). The ability to facilitate leukocyte adhesion to the stromal cells implies that α4β1 integrin/VCAM-1 interactions is an important factor in the initiation of early B cell development (Miyake et al. 1992). Several studies have highlighted the capacity of α4β1 integrin/VCAM-1

[1]To whom correspondence should be addressed: e-mail address: kondoa@glycot.med.osaka-u.ac.jp

Table I. Primer sequences used in real-time PCR

Vpreb1	Forward	5′-CGTCTGTCCTGCTCATGCT-3′
	Reverse	5′-ACGGCACAGTAATACACAGCC-3′
Tcfe2a	Forward	5′-TCCTTTGACCCTAGCCGGACATAC-3′
	Reverse	5′- CCAACACTGGTGTCTCTCCCAAAG-3′
Ebf1	Forward	5′-CCATCCGAGTTCAGACACCTCCT-3′
	Reverse	5′-ACCTCTGGAAGCCGTAGTCGATG-3′
Pax5	Forward	5′-CGCGTGTTTGAGAGACAGCACTACT-3′
	Reverse	5′-GTCTCGGCCTGTGACAATAGGGTAG-3′
Cd79a	Forward	5′-ACCGCATCATCACAGCAGAAGG-3′
	Reverse	5′-TCCTGGTAGGTGCCCTGGA-3′
Cd79b	Forward	5′-GCTGTTGTTCCTGCTGCTGC-3′
	Reverse	5′-CTTCACCATGGAGCTCCGCTTT-3′
GAPDH	Forward	5′-AAATGGTGAAGGTCGGTGTG-3′
	Reverse	5′-TGAAGGGGTCGTTGATGG-3′

interactions to mediate strong adhesion within a model of leukocyte trafficking and enhance activation (van Dinther-Janssen et al. 1991; Carrasco and Batista 2006). Pre-B cell integrins and their stromal cell ligands, together with pre-B cell receptor (preBCR) and galectin-1, form a homogeneous lattice at the contact area between pre-B and stromal cells (Rossi et al. 2006). Springer's group (Carman and Springer 2004) has shown that VCAM-1 is associated with actin-rich microvilli in the "cup-like" structure, and has suggested that this provides directional guidance to leucocytes for extravasation.

Previous reports showed that the functions of integrins were regulated by *N*-glycans catalyzed by *N*-acetylglucosaminyltransferase III (GnT-III), GnT-V, sialyltransferases etc. (Yamamoto et al. 2001; Guo et al. 2002; Pochec et al. 2003). The introduction of bisecting GlcNAc into α5β1 integrin was recently shown to down-regulate cell adhesion, ligand affinity, and cell migration (Isaji et al. 2004). More recently, impaired α3β1 integrin-mediated cell migration was found in $Fut8^{-/-}$ embryonic fibroblasts (Zhao et al. 2006). Based on the amino acid sequences, α4β1 integrin contains 11 and 12 potential asparagine-linked glycosylation sites on each of the α4 and β1 subunits, respectively. There are seven potential *N*-linked glycosylation sites in the immunoglobulin-like domains of VCAM-1 (Vonderheide et al. 1994). Given the various biological functions of *N*-linked glycosylation, the function of the core fucose of α4β1 integrin and VCAM-1 deserves a more detailed investigation. In particular, the function of core fucose associated with α4β1 integrin/VCAM-1 interactions in B cell development has not yet been investigated.

In the present study, we show that core fucosylated *N*-glycans were required for functional α4β1 integrin/VCAM-1 interactions to support B cell development. Pre-B cell colony formation was attenuated due to the lowered α4β1 integrin/VCAM-1-mediated interaction of pre-B cells and stromal cells by the loss of core fucose. These findings clearly demonstrate the crucial role of *Fut8* in early B lymphopoiesis.

Results

Disruption of Fut8 led to B lymphopoietic failure at the pre-B cell stage

We first focused on the differentiation of hemato-lymphopoietic cells by *Fut8* deficiency. Flow cytometry analysis revealed that, while $CD45R^+CD43^+$ (pro-B enriched) population was sustained, $CD45R^+CD43^-$ (pre-B enriched) and $CD45R^+IgM^+$ (immature B enriched) population were significantly reduced in $Fut8^{-/-}$ BM (Table II and representative data in Figure 1). $CD45R^+CD43^-$ (pre-B) and $CD45R^+IgM^+$ (immature B) cells comprised 17.8 ± 4.5% and 4.7 ± 0.8% of the $Fut8^{-/-}$ BM, while those of control littermates were 30.2 ± 2.6% and 7.8 ± 1.7%, respectively. However, no significant difference was found in the frequency of the $CD45R^+CD43^+$ (pro-B) cell population between the $Fut8^{+/+}$ and $Fut8^{-/-}$ mice (Table II). Flow cytometry analysis of the spleen subsequently revealed that the frequency of $CD45R^+IgM^+$ cells was significantly reduced in $Fut8^{-/-}$ mice, whereas those of $CD11b^+$ myeloid cells and the $TER119^+$ erythroid cells were increased (Table II). In contrast to the significant change of early B cell populations, development of $CD4^+$ or $CD8^+$ T cells, natural killer cells and natural killer T cells were relatively normal in the $Fut8^{-/-}$ mice (Table II). These findings implied that *Fut8* expression is required for pro-B cells to properly differentiate to pre-B and later stages of B cell development.

It is noteworthy that the FUT8 product, a core fucosylated *N*-glycan, is ubiquitously expressed in the BM microenvironment of $Fut8^{+/+}$ BM but not in $Fut8^{-/-}$ mice. There was no difference in apoptosis, as evidenced by Tunel staining has been found between $Fut8^{+/+}$ and $Fut8^{-/-}$ mice (Figure 2). A selective and profound reduction in the pre-B and immature B cell populations, and no concomitant change in the population

Table II. Comparison of BM cell, splenic cell, and thymic cell compositions analyzed by four-color FACS between $Fut8^{+/+}$ and $Fut8^{-/-}$ mice

Genotype		$Fut8^{+/+}$ mice	$Fut8^{-/-}$ mice	
BM	$CD45R^+CD43^+$ (%) (pro-B enriched)	6.9 ± 2.6	6.2 ± 2.6	$P > 0.05$
	$CD45R^+CD43^-$ (%) (pre-B enriched)	30.2 ± 2.6	17.8 ± 4.5	$P < 0.01$**
	$CD45R^+IgM^+$ (%) (immature B enriched)	7.8 ± 1.7	4.7 ± 0.8	$0.01 < P < 0.05$*
	$CD11b^+$(%) (myeloid)	27.2 ± 7.6	28.9 ± 4.9	$P > 0.05$
	$TER119^+$(%) (erythroid)	48.5 ± 15.9	65.6 ± 11.5	$P > 0.05$
Spleen	$DX5^+CD3^-$ (%)	2.4 ± 0.5	2.5 ± 0.5	$P > 0.05$
	$DX5^+CD3^+$ (%)	1.5 ± 0.5	1.3 ± 0.2	$P > 0.05$
	$CD4^+CD3^+$ (%)	6.5 ± 4.1	7.2 ± 7.5	$P > 0.05$
	$CD8^+CD3^+$ (%)	4.4 ± 5.7	5.2 ± 8.2	$P > 0.05$
	$CD45R^+IgM^+$ (%)	16.4 ± 3.3	9.9 ± 3.1	$0.01 < P < 0.05$*
	IgM^+IgD^- (%)	8.1 ± 2.4	4.8 ± 1.2	$0.01 < P < 0.05$*
	$CD11b^+$ (%)	6.2 ± 0.5	10.4 ± 0.8	$P < 0.01$**
	$TER119^+$(%)	28.5 ± 3.5	41.7 ± 4.1	$P < 0.01$**

Data are representative of the mean ± SD of four mice per genotype. *$P < 0.05$; **$P < 0.01$.

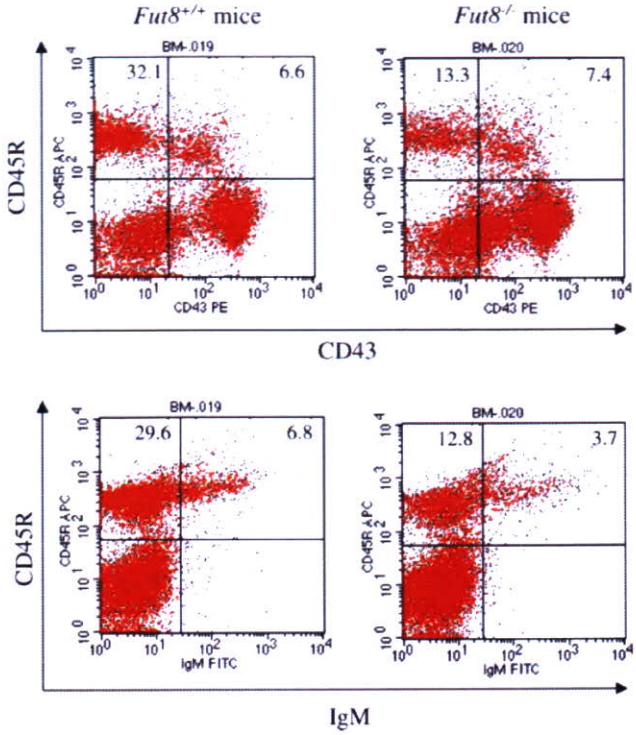

Fig. 1. FACS analysis of the proportion of $CD45R^+CD43^-$, $CD45R^+IgM^-$, and $CD45R^+IgM^+$ cells in the *Fut8*$^{-/-}$ BM. Numbers indicated in the top corners represent the percentage of total BM cells. Quadrants were set and 10,000 events were acquired for each analysis. The results of one representative experiment of four are shown.

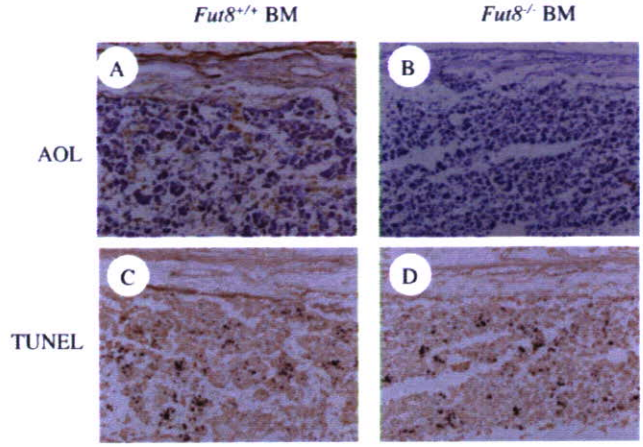

Fig. 2. Immunohistochemical staining of BM. Sections from 2-week-old mice were stained with AOL and TUNEL. Panels A and B indicate BM of *Fut8*$^{+/+}$ and *Fut8*$^{-/-}$ mice stained with AOL. Panels C and D indicate BM of *Fut8*$^{+/+}$ and *Fut8*$^{-/-}$ mice stained for TUNEL. Experimental conditions are described in Materials and methods. The magnification is $\times 100$.

containing pro-B cells were observed in the *Fut8*$^{-/-}$ BM (Figure 1). These results suggest that the *Fut8* defect results in impaired pre-B cell expansion, which is not due to any accelerated apoptosis.

Loss of Fut8 reduced the frequency of pre-B cells supported by stromal cells

To address the abnormality of the pro-B to pre-B transition in *Fut8*$^{-/-}$ mice, fractions containing $CD45R^+CD43^+$, $CD45R^{low}CD43^-$, $CD45R^+IgM^-$, and $CD45R^+IgM^+$ cells in the BM were sorted, and the expression of *Fut8* in these fractions were examined by real-time polymerase chain reaction (PCR). All of these B progenitor fractions expressed the *Fut8* gene and the developmental progression from pro-B to the pre-B cell stage was accompanied by an increase in the RNA expression level of *Fut8* (Fig. 3). The results further support the hypothesis that *Fut8* plays important roles in the pro-B to pre-B cell transition, and that the targeting of *Fut8* consequently lead to B lymphopenia beyond the pro-B cell stage.

We then performed colony assays to compare the frequencies of the B cell progenitors defined by their growth requirement between *Fut8*$^{+/+}$ BM and *Fut8*$^{-/-}$ BM cells. In the *Fut8*$^{-/-}$ BM, the frequency of clonable pre-B cell progenitors in the presence of stromal cells (ST2, PA6) and IL-7 declined, compared to those of control littermates (Table III). Furthermore, we found that *Fut8*$^{-/-}$ $CD45R^+IgM^-$ fraction contained significantly less clonable pre-B cells compared to *Fut8*$^{+/+}$ cells (Figure 4A). In contrast, colony formation of pre-B cells in complete methylcellulose medium in response to IL-7 alone (CFU-IL-7) was indistinguishable between *Fut8*$^{+/+}$ pre-B cells and *Fut8*$^{-/-}$ pre-B cells (Figure 4B). These results strongly indicate that *Fut8* expression in pre-B progenitor is important for their growth through pre-B cells/stromal cells interaction, but not IL-7 reactivity.

It is noteworthy that the frequency of pre-B cell progenitors on PA6 was significantly lower than those on ST2 (Table III). We also found that the FUT8 protein was much lower in PA6

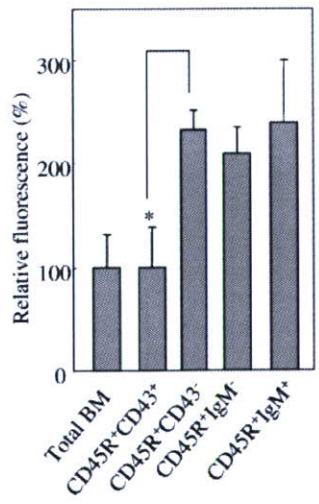

Fig. 3. *Fut8* expression is increased during the pro-B to pre-B transition. The $CD45R^+CD43^+$, $CD45R^{low}CD43^-$, $CD45R^+IgM^-$, and $CD45R^+IgM^+$ cells were gated and sorted from two-week-old *Fut8*$^{+/+}$ mice. Sorted cell populations were routinely reanalyzed and showed more than 90% purity, respectively. *Fut8* gene expression of sorted $CD45R^+CD43^+$, $CD45R^{low}CD43^-$, $CD45R^+IgM^-$, and $CD45R^+IgM^+$ cell fractions by real-time PCR. Total BM cells were prepared prior to sorting. Data are representative of three experiments. $^*P < 0.05$.

Table III. Frequency of colonies of $Fut8^{+/+}$ BM cells and $Fut8^{-/-}$ BM cells in response to stromal cells (ST2 or PA6) and IL-7

	No. of colonies per plate (frequency)	
	$Fut8^{+/+}$ mice	$Fut8^{-/-}$ mice
ST2 + IL-7-dependent precursors	45.4 ± 6.2 (1/78)	29.4 ± 2.4 (1/138)*
PA6 + IL-7-dependent precursors	26.6 ± 5.0 (1/154)	11.4 ± 3.0 (1/398)*

BM cells, sorted from two-week-old mice, were cultured in 96-well plates in RPMI 1640 medium containing 10 ng/mL recombinant human IL-7. The inoculum size was 50 cells per well. Colonies were counted after seven days of culture.

cells by Western blot, compared to ST2 cells that strongly expressed (Figure 5A). To further clarify the involvement of *Fut8* of stromal cells for the growth of B progenitor cells, we stably knocked down the *Fut8* gene of ST2 cells, referred to as ST2-KD. No apparent changes were found in the expressions of other glycosyltransferase genes, such as GnT III and β1,4-galactosyltransferase I (β4GalT-I) (data not shown). As shown in Figure 5B, the introduction of *Fut8* siRNA successfully suppressed FUT8 expression. An *Aspergillus oryzae* lectin (AOL) blot analysis confirmed the effective knockdown of FUT8 expression (Figure 5C). To determine whether the core fucosylated *N*-glycans of ST2 cells functionally compromised pre-B cell colony formation, we cultivated $Fut8^{+/+}$ BM cells on ST2 cells and on ST2-KD cells. The frequency of B cell progenitors was 1/251 on ST2-KD cells, which was less than half of that on ST2 cells (1/114) (Figure 5D). These results indicate that *Fut8* in BM stromal cells is involved in pre-B supporting ability.

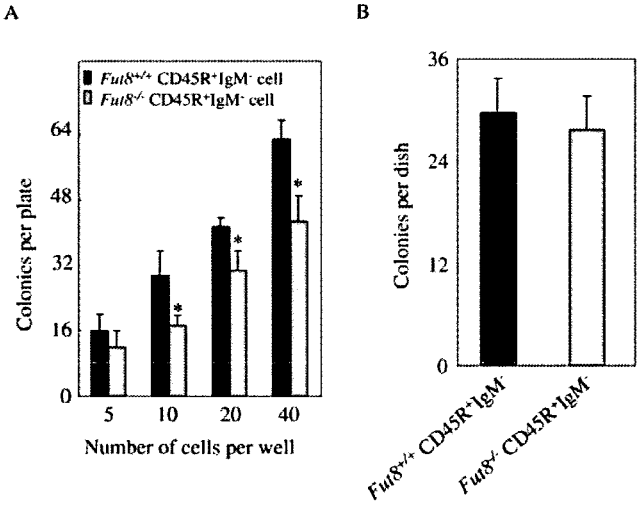

Fig. 4. Comparison of the frequencies of pre-B cells between $Fut8^{+/+}$ $CD45R^+IgM^-$ cells and $Fut8^{-/-}$ $CD45R^+IgM^-$ cells in response to ST2 cells + IL-7 (**A**) or IL-7 alone (**B**). $CD45R^+IgM^-$ pre-B cells were isolated using the MACS magnetic cell sorting system with anti-CD45R-conjugated microbeads after depletion with anti-IgM-conjugated microbeads. In (**A**), pre-B colonies counted were cultured for seven days in the presence of IL-7 and stromal cells. In (**B**), pre-B colonies counted were cultured for seven days in the complete methylcellulose medium in the presence of IL-7. Data are presented as the mean ± SD of pre-B colony-forming units. All assays were performed in triplicate.

Ablation of core fucose of VCAM-1 and α4β1 integrin lowered binding ability of pre-B cells to ST2 and VCAM-1 molecule

It is well known that α4β1 integrin/VCAM-1 interactions are involved in facilitating B cell adhesion to stromal cells and in enhancing B cell activation (Carrasco et al. 1992). Indeed, colony formation of BM cells on ST2 cell with IL-7 was completely blocked by treatment with 10 μg/mL of an anti-VCAM-1 antibody or an anti-α4β1 integrin antibody (Figure 5D). Thus, we analyzed the effect of core fucose on α4β1 integrin and VCAM-1 in the adhesion of pre-B cells to stromal cells. To ascertain the role of the core fucose of VCAM-1, we compared the binding ability of $Fut8^{+/+}$ pre-B cells with that of ST2 and ST2-KD cells. The core fucosylated *N*-glycans of VCAM-1 was abolished in ST2-KD cells without any effect on the total VCAM-1 expression levels (Figure 6A). As shown in Figure 6B, the $Fut8^{+/+}$ pre-B cells showed a weaker adhesion to ST2-KD, indicating that FUT8 in stroma has positive role in tethering pre-B cells. On the other hand, $Fut8^{-/-}$ pre-B cells showed weaker binding to ST2-KD than $Fut8^{+/+}$ pre-B cells. Furthermore, when the recombinant mouse VCAM-1/Fc chimera was used, binding of $Fut8^{-/-}$ pre-B cells was weaker than that of $Fut8^{+/+}$ pre-B cells, suggesting that the adhesion of pre-B cells themselves by α4β1 integrin was also impaired by defect of FUT8 in pre-B cells.

To further examine the importance of the core fucosylated *N*-glycans on α4β1 integrin, we stably silenced *Fut8* expression in a pre-B cell line, 70Z/3 cells, and named 70Z/3-KD. As shown in Figure 6C and D, FUT8 expression and the core fucosylated *N*-glycans of α4β1 integrin were ablated in 70Z/3-KD. Reintroduction of the *Fut8* gene into 70Z/3-KD cells restored the core fucosylation of α4β1 integrin (70Z/3-KD-re). No significant differences in the expression levels of α4β1 integrin on the cell surface were found among the three cell types (Figure 6D). In a binding assay, 70Z/3-KD cells showed an impaired adhesion to VCAM-1, compared to mock cells. Preincubation of 70Z/3 cells with an anti-α4β1 integrin antibody significantly blocked the binding of 70Z/3 to VCAM-1. The reintroduction of *Fut8* restored the binding, as evidenced by an increase in the percentage of binding cells from 30 to 45% (Figure 6E), indicating that core fucosylated *N*-glycans are required for functional α4β1 integrin/VCAM-1 interactions to support B cell development. Collectively, these results demonstrated that core fucosylation plays a pivotal role in a key event in pre-B cell development; α4β1 integrin/VCAM-1-mediated interactions between pre-B cells and stromal cells.

Pre-B cells in $Fut8^{-/-}$ mice exhibit a reduced gene expression critical for early B cell development

Completing the productive rearrangement of immunoglobulin μ heavy chain gene in B progenitor cells Igμ chain associates with the surrogate light chain (SLC), which is composed of λ5 and VpreB (encoded by *Vpreb1*) proteins, and the CD79a (Igα))/CD79b (Igβ) transducing complex, to form the preBCR complex. To address the underlying molecular mechanism of the impaired pre-B cell generation, we examined the pattern of gene expression in $Fut8^{-/-}$ pre-B cells by real-time PCR. We found that the expression of *Tcfe2a*, *Ebf1*, *Cd79a*, and *Cd79b* in $Fut8^{-/-}$ pre-B cells was lower than that in $Fut8^{+/+}$ pre-B cells, by a decrease of 45.9%, 80.9%, 23.3%, and 53.6% relative to $Fut8^{+/+}$ cells, respectively, with no change in *Pax5* and

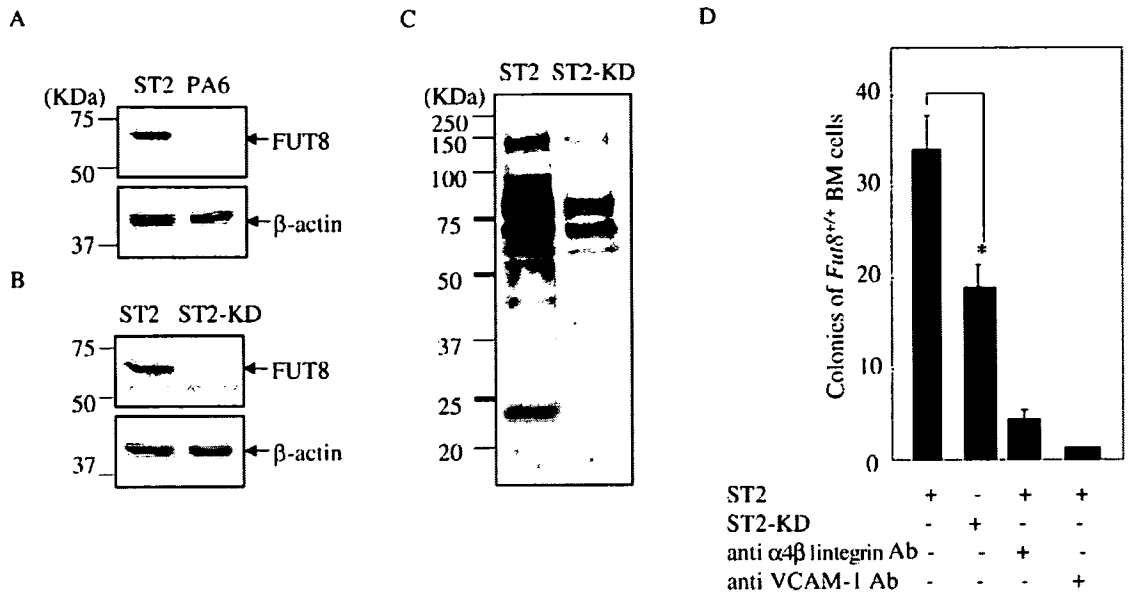

Fig. 5. Characterization of ST2 and PA6 cells. (**A**) Comparison of FUT8 expression between ST2 and PA6. Western blots for *Fut8* expression probed with a mouse monoclonal antibody 15C6, which recognizes FUT8 in a 12.5% gel. (**B**) Gene-silencing effects of siRNA on the *Fut8* expression were determined by Western blot. Expression of β-actin is shown as loading control. (**C**) Core fucosylated *N*-glycans are probed with AOL in 10% gel. (**D**) *Fut8* ablation leads to reduced pre-B cell colony formation. $^*P < 0.05$.

Vpreb1 expression (Figure 7A). The surface expression preBCR and CD79b on $CD45R^{low}CD43^-$ cells was further analyzed by flow cytometry. The percentage of $Fut8^{-/-}$ $preBCR^+CD79^{low}$ cells was 2.4% of the pre-B cells, whereas that of $Fut8^{+/+}$ $preBCR^+CD79^{low}$ cells was 4.4% (Figure 7B). These results suggest that pre-B cell differentiation of $Fut8^{-/-}$ mice is impaired at the step where B progenitors expressing the preBCR complex on their surface is generated.

Discussion

In the present study, we found that targeting of $Fut8^{-/-}$ resulted in the reduction of wide range of B-lineage cells. Using techniques of flow cytometry, colony assays, and quantitative RT-PCR, we revealed that the transition from pro-B to pre-B cells is affected by the deficiency of FUT8. Moreover, a lack of core fucosylated *N*-glycans of α4β1 integrin and VCAM-1 led to a reduction in adhesion between pre-B cells and stromal cells. Since an important role for this interaction in early B-cell development was established, we attributed this reduced interaction to the impaired development of B lymphocytes.

The physiological importance of the fucose modification of proteins has been highlighted by a leukocyte adhesion deficiency II (LAD II) (Luhn et al. 2001), which is categorized in congenital disorder of glycosylation (CDG) genetic disease and is caused by reduced GDP-fucose. In LADII patients, a leukocyte adhesion is reduced due to a deficit in selectin-mediated adhesion through fucosylated ligands, such as sialyl Le^x. As previously reported, FUT8 is able to modify multiple glycoproteins and affect their functions. Core fucosylation could affect the conformation and flexibility of the antenna of N-linked biantennary oligosaccharides (Stubbs et al. 1996). The binding affinities of the TGF-β type II receptor and/or EGF receptor for their respective ligands are reduced in $Fut8^{-/-}$ cells (Wang et al. 2005; Li et al. 2006; Wang et al. 2006), suggesting that the core fucose is involved in ligand binding and the subsequent activation of various receptors (Kondo et al. 2006; Taniguchi et al. 2006). It has also been reported that the increase of *Fut8* activity in megakaryocytes (MKs) progenitors preceded the increase of $CD41a^+$ cell generation (Bany-Laszewicz et al. 2004). In the present study, we found that a deficiency in core fucosylation caused an abnormality in the immune system, particularly in B cell development.

α4β1 integrin binds to fibronectin and VCAM-1 expressed by stromal cells in the BM microenvironment (Miyake et al. 1991), mediates interactions of cell-extracellular matrix proteins as well as cell–cell interactions. α4β1 integrin binds to domain 1 or domain 4 of VCAM-1, involving amino acids within the linear sequence Q-I-D-S-P-L, which is expressed in each domain (Vonderheide and et al. 1994). Although integrin-mediated adhesion is based on the binding of α and β subunits to a defined peptide sequence, the strength of this binding is modulated by various mechanisms such as posttranslational glycosylation (Gu 2004). There is an evidence to show that glycosylation alters β1 integrin function (Wadsworth et al. 1993). In addition, it has been reported that murine β1 integrins deficient in glycosylation show a reduced affinity for fibronectin and laminin (Oz et al. 1989). Moreover, impaired α3β1 integrin-mediated cell migration was found in $Fut8^{-/-}$ embryonic fibroblasts (Zhao et al. 2006). Our results showed that the ability of 70Z/3 cells to bind a VCAM-1 chimera was significantly attenuated by the knockdown of *Fut8* expression, and that the reintroduction of *Fut8* restored this binding ability (Figure 6E). The binding of $Fut8^{-/-}$ pre-B cells to ST2 and VCAM-1 was also decreased, compared with $Fut8^{+/+}$ cells (Figure 6B), suggesting that core fucosylated *N*-glycans involved in pre-B cell and stromal cell interactions. Since both α4β1 integrin and VCAM-1 are

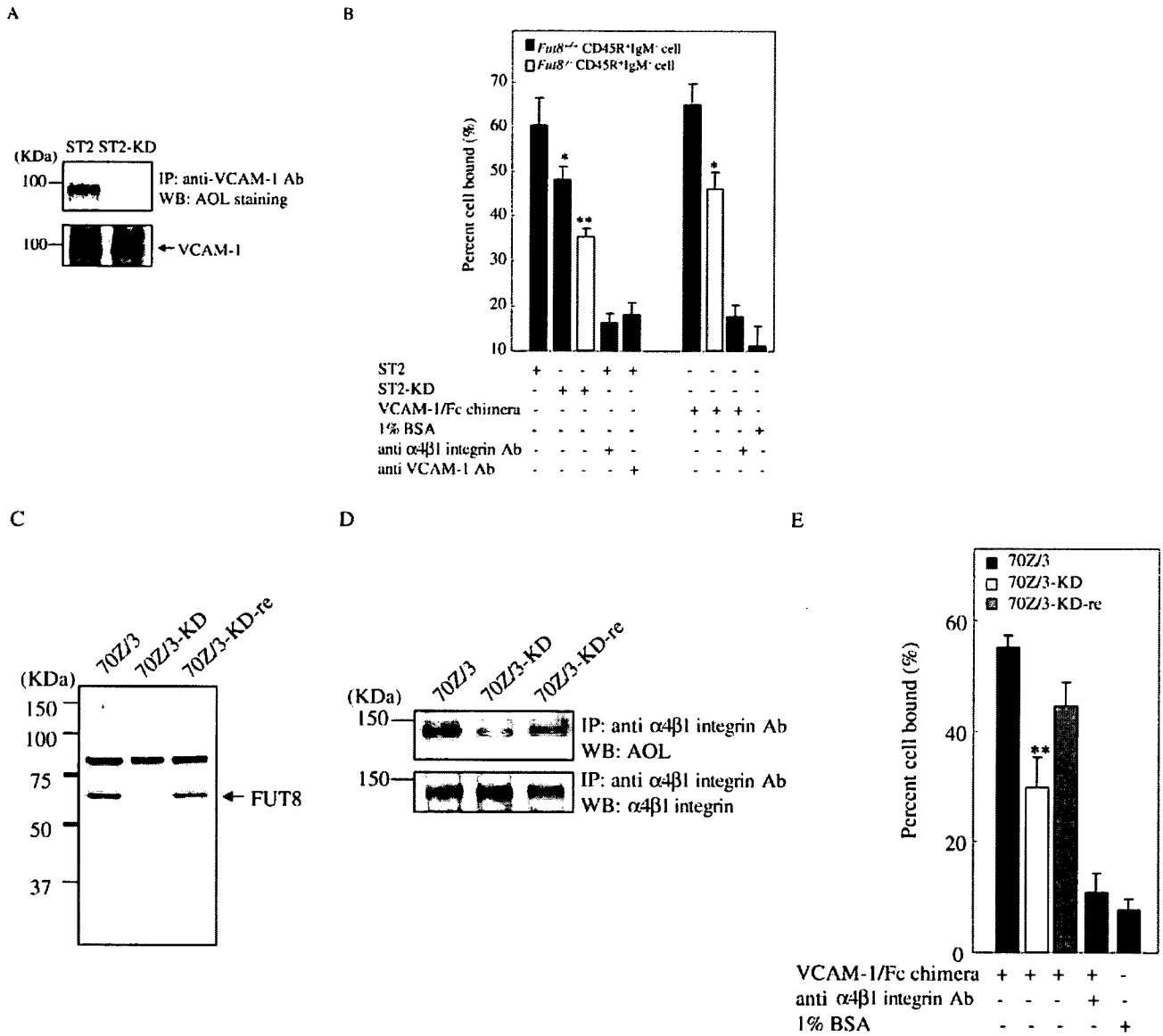

Fig. 6. Loss of core fucose on VCAM-1 and α4β1 integrin led to a low binding ability of pre-B cells to ST2 and VCAM-1 molecules. (**A**) Reduction in the core fucose of VCAM-1 in ST2-KD was detected by AOL staining. An antibody to VCAM-1 was used in the immunoprecipitation and the immunoprecipitates were resolved by SDS-PAGE on a 7.5% gel, transferred to a PVDF membrane and probed with the AOL and anti-VCAM-1. The immunoprecipitates were treated with Laemmli sample buffer containing 2-ME. (**B**) Inhibition of binding of $CD45R^+IgM^-$ cells to ST2 and VCAM-1 molecules as the result of de-core fucosylation. Quantification of cell numbers attached to the plates was carried out by means of fluorescence microassay. $CD45R^+IgM^-$ cells were GFSE labeled and used in the cell adhesion assay as described in Materials and methods. $^*P < 0.05$; $^{**}P < 0.01$. (**C**) Expression of FUT8 on 70Z/3 derivative cells. Ten μg of cell lysates from 70Z/3, 70Z/3-KD and 70Z/3-KD-re cells were subjected to a western blot analysis using 15C6 antibody. (**D**) Reduction in core fucose of α4β1 integrin in 70Z/3-KD was detected by AOL staining. The surfaces of 70Z/3, 70Z/3-KD and 70Z/3-KD-re cells were biotinylated, and whole cell lysates were immunoprecipitated with an anti-α4β1 integrin antibody. The immunoprecipitates were treated with Laemmli sample buffer without 2-ME. (**E**) Comparison of the binding ability of 70Z/3, 70Z/3-KD, and 70Z/3-KD-re cells to VCAM-1 molecules. The binding ability of pre-B cells was evaluated by counting the number of B cells bound per well. Monoclonal antibodies (10 μg/mL) to α4β1 integrin and VCAM-1 were added as indicated. Adherence is expressed as a percentage. Each value represents the mean ± SD of three experiments. $^{**}P < 0.01$.

heavily *N*-glycosylated (Vonderheide et al. 1994), it is very likely that core fucosylation affects α4β1 integrin/VCAM-1 interaction. The increasing affinity of integrins for their extracellular ligands, i.e., integrin activation, is controlled by conformational changes in the extracellular domains from an inactive to active form (Calderwood 2004). The lack of core fucose might cause conformational changes in the extracellular domains of integrin, subsequently affecting α4β1 integrin/VCAM-1 interactions. The phenotype of $Fut8^{-/-}$ mice combined with our in vitro data presented an intriguing possibility that core fucose is involved in the appropriate interactions of pre-B cells and stromal cells.

The important roles for α4β1 integrin/VCAM-1 interactions in early B cell development were demonstrated in vitro (Miyake

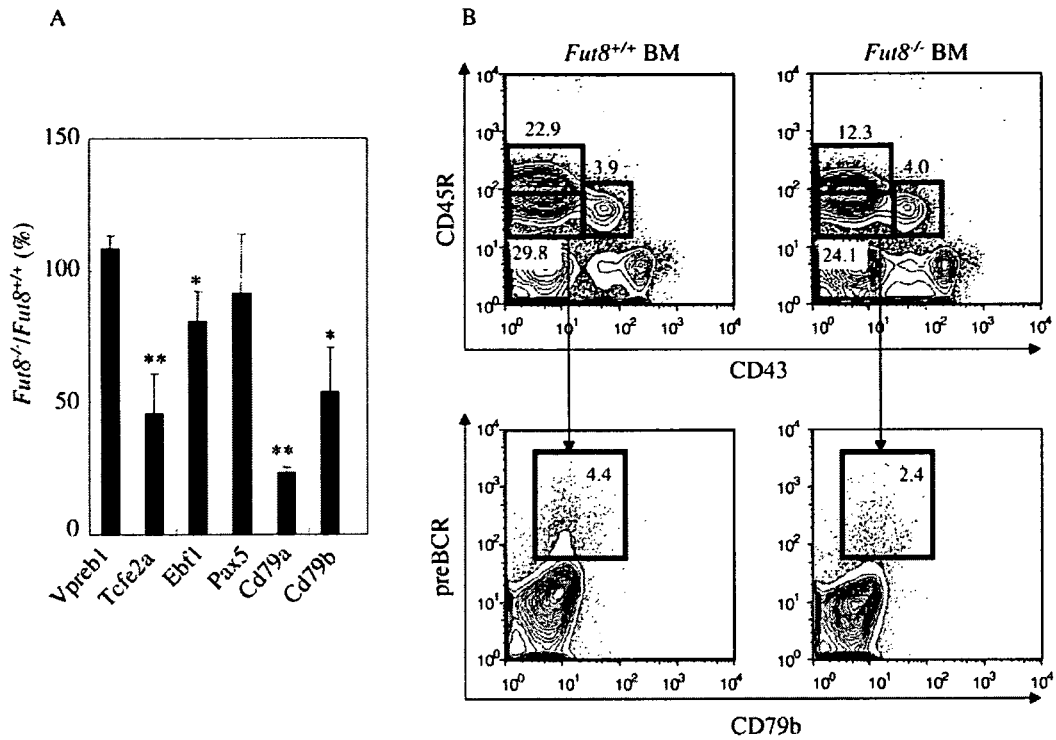

Fig. 7. (**A**) Real-time PCR analysis of *Fut8*$^{-/-}$ CD45R^{+}IgM^{-} gene expression. RNAs were isolated from CD45R^{+}IgM^{-} cells of *Fut8*$^{+/+}$ and *Fut8*$^{-/-}$ mice. Three mice of each genotype were analyzed. All values were normalized to that of the GAPDH gene and are presented as a ratio relative to that of *Fut8*$^{+/+}$ (set as 100%). $^{*}P < 0.05$; $^{**}P < 0.01$. (**B**) Impaired generation of preBCR^{+} cells in *Fut8*$^{-/-}$ CD45R^{low}CD43^{-} pre-B cells. Numbers adjacent to the boxed areas indicate the frequency of cells in each as a percentage of the total BM cells. The numbers in boxes indicate percentage of preBCR^{+}CD79^{low} cells. Data were analyzed using the FLOWJO software program.

et al. 1991). Here, the core fucose of α4β1 integrin and VCAM-1 was found to be important in α4β1 integrin/VCAM-1 interactions that could account for the decreased development of B cell progenitors in response to stromal cells and IL-7. First, the extent of B cell colony formation on ST2-KD cells in the presence of IL-7 was much less than on parent ST2 cells (Figure 5D), indicating that core-fucosylation of VCAM-1 was required for full ability of stromal cells to support pre-B cells. Second, a significant decrease was observed in the frequencies of clonable pre-B cells in *Fut8*$^{-/-}$ CD45R^{+}IgM^{-} cells as compared with *Fut8*$^{+/+}$ CD45R^{+}IgM^{-} cells (Figure 4A), suggesting that core fucose of pre-B cells is also required for receiving the growth-supporting signals from stromal cells. The impaired signal was not IL-7-mediated, because CFU-IL-7 was not altered in *Fut8*$^{-/-}$ CD45R^{+}IgM^{-} cells. Finally, 70Z/3-KD showed significantly decreased adhesion to the VCAM-1/Fc chimera molecule, indicating that adhesion of α4β1 integrin on pre-B cells was also impaired by loss of core fucosylation. Collectively, it is reasonable to conclude that the low α4β1 integrin/VCAM-1 interaction caused the impaired pre-B cell development in *Fut8*$^{-/-}$ mice. Given the appropriate α4β1 integrin/VCAM-1 interaction enables pre-B cells to communicate with stromal cells, it would be interesting to see the changes of early B- related gene expressions by the communication.

In this context, our analyses provide the suggestive evidence that the gene expressions crucial for transition from pro-B cells to pre-B cells are affected by *Fut8* deficiency. Early B cell development is controlled by a hierarchical regulatory network that induces several key transcription factors, such as PU.1, Ikaros, E2A (encoded by *Tcfe2a*), EBF (encoded by *Ebf1*), and Pax5 (Singh et al. 2005). Interestingly, quantitative real-time PCR analyses revealed that *Fut8*$^{-/-}$ pre-B cells express lower transcriptional genes such as *Ebf1* and *Tcfe2a*, which promote the activation of B cell. Single and dual knockout mice showed that EBF1 and E2A proteins collaborate to activate the expression of early B cell genes such as *CD79a, B29, Vpre-B, λ5, RAG-1*, and *RAG-2*. Mice lacking the E2A showed defective B lymphopoiesis similar to that of *Ebf*$^{-/-}$ mice (Zhuang Soriano et al. 1994; Lin and Grosschedl 1995). Similar to E2A- or EBF-deficient mice, *Pax5*$^{-/-}$ mice exhibited an early block of B cell differentiation, but at a slightly later stage (pre-BI) (Urbanek Wang et al. 1994). Interestingly, recent research reported that *Fut8* expression was increased in pro-B cells lacking Pax5, which is an indispensable transcription factor for lineage decision to B lymphocytes (Deloguet al. 2006). Although it is difficult to determine the blocked step precisely by using materials with heterogenous populations, the step of transition from pro-B cells to pre-B cells seems to be a vulnerable point affected by *Fut8* deficiency. The combined down-regulation of those genes, *CD79a, CD79b, Ebf1*, and *Tcfe2a* in *Fut8*$^{-/-}$ B progenitors is likely to be the most crucial effect resulted from the impaired α4β1 integrin/VCAM-1 interactions.

Overall, the most important finding of this study is the significant decrease in pre-B cells in the *Fut8*$^{-/-}$ BM, which provides an intriguing evidence that a core fucose moiety is critically important in pre-B cell development. FUT8 modulates α4β1

integrin/VCAM-1 interactions during B cell development and could regulate pre-B cell repopulation via the down-regulation of B cell related genes. Our study provides new insights into the biological functions of the core fucose during B cell development and provides a hint for elucidation of B cell related diseases, agammaglobulinaemia and lymphoma.

Materials and methods

Mice

BALB/cA mice were purchased from the Charles River Laboratories Japan (Yokahama, Japan). *Fut8*$^{-/-}$ mice were generated as previously described (Wang et al. 2005), and had been backcrossed eight times to the BALB/cA background. Homozygous wild (*Fut8*$^{+/+}$) and knockout (*Fut8*$^{-/-}$) mice were obtained by crossing heterozygous *Fut8*$^{+/-}$ mice. *Fut8*$^{-/-}$ and control wild-type (*Fut8*$^{+/+}$) mice in the same littermate were analyzed at around two weeks of age. All animal procedures complied with the institutional animal protocol guidelines.

Antibodies

FITC-labeled anti-CD4 (GK1.5), anti-IgM (11/41), anti-erythroid (TER-119), anti-NK cells (DX5), anti-CD79b (HM79–16), anti-IgD (11–26), anti-CD43 (S7), anti-Gr-1 (RB6–8C5), APC-labeled anti-CD11b (Mac-1, M1/70), anti-CD45R (RA3–6B2), anti-CD8 (53–6.7) were obtained from e-Bioscience. Additional biotin-conjugated anti-preBCR antibody (SL156) and streptavidin-PE Cy5 were purchased from BD Bioscience (Franklin Lakes, NJ). A mouse monoclonal antibody for rat/mouse β-actin (sc-8432) was purchased from Santa Cruz (Santa Cruz, CA); a mouse monoclonal anti-FUT8 antibody (15C6) was obtained from Fujirebio Inc. (Shinjuku, Japan); a rat anti-VCAM-1 IgG_{1k} antibody (M/K-2) was from SouthernBiotech (Birmingham, AL); a rat anti-mouse CD49 (PS-2) antibody was from Serotec Ltd. (Oxford, U.K.); a rabbit anti-mouse IgG HRP-conjugate was from ICN Pharmaceuticals, Inc. (Arora, OH); a donkey anti rat IgG HRP-conjugate was from Beckman Coulter, Inc. (Fullerton, CA).

Cell purification

The BM cells were obtained by crushing two femurs and two tibia of two-week-old mice. The crude mixture was filtered through nylon mesh, and resuspended at 1×10^7 cells per mL. Single-cell suspensions of the spleens and thymi were prepared by first grinding the tissues with frosted slides, and then by gentle passage through the nylon mesh. These cells were resuspended at 1×10^7 cells per mL. Red blood cells were lysed by incubation with 0.14 M NH_4Cl and 20 mM Tris (pH 7.4) for 3 min at room temperature. In experiments using enriched pre-B cells, IgM^+ cells were depleted from BM cells, and then $CD45R^+$ cells were positively sorted with antibody-conjugated magnetic beads (Miltenyi Biotec, Bergish Gladbach, Germany). The sorted $CD45R^+IgM^-$ cell populations were routinely >96% pure by fluorescence activated cell sorting (FACS) analysis.

Cell culture conditions

The 70Z/3 cells, a pre-B lymphoma line, were obtained from Dr. Paul W. Kincade. The stromal cell lines, ST2 and PA6 were from Dr. S-I Hayashi. All cell lines were grown in RPMI 1640 supplemented with 2 mM glutamine, 50 μM 2-mercaptoethanol (2-ME) (Fluka, Buchs, Switzerland), 5% FCS, 100 U/mL penicillin, 100 μg/mL streptomycin. In some experiments, the indicated concentration of recombinant mouse IL-7 (Sigma) was added.

Flow cytometry and cell sorting

For phenotypic analysis, the BM cells were first incubated with an anti-CD16/CD32 (2.4G2) mAb to block Fc receptors, and then stained on ice for 15 min with several combinations of mAbs, as indicated in the figure legends. Flow cytometry was performed on a FACS-Calibur (Becton Dickinson, Mountain View, CA), and the data were analyzed with the CellQuest (Becton Dickinson) or Flowjo software (Treestar, San Carlos, CA).

For cell sorting, BM cells were stained with FITC-labeled anti-IgM, PE-labeled anti-CD43, APC labeled anti-CD45R, and subpopulations were sorted with a FACStar Plus (Becton Dickinson) instrument.

Assays for B cell progenitors

The frequencies of B cell progenitors growing dependent on stromal cells + IL-7 (clonable pre-B cells) and that on IL-7 alone (CFU-IL-7) were evaluated by means of clonable pre-B cell assay and CFU-IL-7 assay, respectively. For the clonable pre-B cell assay, a monolayer of BM stromal cells such as ST2 and PA6 was allowed to form in 96-well plates (Falcon, Oxnard, CA). The total BM cells and purified $CD45R^+IgM^-$ cells, diluted to the cell number as indicated in the figure legends, were inoculated into the plates. Cells were cultured in RPMI 1640 supplemented with 5% FCS, 50 μM 2-ME, 2 mM glutamine in the presence of 10 ng/mL of IL-7. After seven days of culture, the outgrowth of pre-B cells was surveyed under a microscope, and the frequencies were then calculated according to the formula; frequency = $\{\ln [T/(T - P)]\}/N$, where N, inoculated cell number/well; T, number of total wells; P, number of wells containing a pre-B cell colony.

For CFU-IL-7, enriched $CD45R^+IgM^-$ cells were seeded into methylcellulose media containing 10 ng/mL recombinant human IL-7 (Stemcell technologies Inc). Colonies were counted after seven days of culture. Aggregates consisting of >40 cells were differentially scored as colonies.

Establishment of Fut8 knockdown cell lines

A retroviral vector carrying siRNA targeted to *Fut8* was constructed as described previously (Li et al. 2006). The targeting sequence of the *Fut8* siRNA used was as follows: sense: 5′ UCU CAG AAU UGG CGC UAU GTT 3′, antisense: 3′ TTAGA GUC UUA ACC GCG AUA C 5′. The ST2 and 70Z/3 derivative cell lines, stably transfected with the plasmid expressing siRNA that targeted FUT8 are referred to hereafter as "ST2-KD" and "70Z/3-KD."

For *Fut8* reintroduction, ORF of FUT8 was cloned into Hpa I site of pLHCX vector (Clontech) To prepare pLHCXsi-mU6-*Fut8* expression vectors resistant to the siRNAs expressed in the *Fut8*-knockdown cells, we introduced multiple mutations into pLHCXsi-mU6-*Fut8* (five point mutations for the *Fut8*–1386-1404 region) that did not alter the original amino acid residues.

Immunohistochemistry

The femurs from *Fut8*$^{+/+}$ mice and *Fut8*$^{-/-}$ mice were dissected and fixed overnight in 10% formaldehyde containing 2% sucrose. The tissues were then decalcified in 0.37% unbuffered formaldehyde containing 5.5% ethylenediamine tetraacetic acid (EDTA) (pH 6.0–6.5) for four days. After fixation and decalcification, the specimens were embedded in paraffin, and 5 μm sections were prepared. The sections were histochemically stained with biotin-conjugated AOL (Ishida et al. 2002), which preferentially recognizes core fucosylation on *N*-glycans. Briefly, sections were deparaffinized twice in xylene and hydrated through a graded series of ethanol to phosphate-buffered saline (PBS). Endogenous peroxidase activity was blocked with 3% H_2O_2 for 5 min. After washing with PBS containing 0.1% Tween 20 (PBS-T), the slides were blocked with an avidin/biotin blocking kit (Vector Laboratories, Burlingame, CA). The slides were incubated with biotin-conjugated AOL, and washed three times with PBS-T. The slides were covered with horseradish peroxidase (HRP)-streptavidin (Vector Laboratories, Peterborough, U.K.) for 30 min. Finally, the slides were visualized with 3, 3′-diaminobenzidine and counterstained with hematoxylin and eosin.

Western blot and lectin blot analysis

The protein samples were electrophoresed with 10% polyacrylamide gels using Mini Protean III electrophoresis tanks (Bio-Rad, Hercules, CA). After the electrophoresis, the proteins were transferred to polyvinylidene difluoride (PVDF) membranes (Immobilon-P, 0.45 μm, Millipore, Bedford, MA,) at 240 mA for 30 min. The blots were blocked for 2 h with 5% skim milk in TBS-T (TBS-T; 10 mM Tris–HCl, pH 7.5, 150 mM NaCl, and 0.1% Tween 20) for immunoblot or with 3% BSA in TBS-T for lectin blot. Following the incubation with the appropriate primary antibodies or AOL overnight, and then the membranes were washed. After washing, the blots were incubated with the corresponding secondary antibodies conjugated with HPR or ABC reagent (Vector Laboratories) for AOL blot. Finally, specific proteins were visualized by using an ECL system (Amersham).

Cell surface biotinylation and immunoprecipitation

The cells were surface labeled by a sulfosuccinimidobiotin (sulfo-NHS-biotin) (Pierce Chemical Co., Rockford, IL) procedure (Miyake et al. 1991). Briefly, after three washes, the cells were suspended in PBS with 0.2 mg/mL of sulfo-NHS-biotin. After 1 h of incubation at 4°C with occasional shaking, the cells were washed three times with chilled PBS. The cell lysates were prepared in lysis buffer containing 50 mM Tris–HCl, 150 mM NaCl, 1% Triton X-100, 2 mM $MgCl_2$, and 2 mM $CaCl_2$, with a protease inhibitor (Nacalai Tesque, Kyoto, Japan) added. After centrifugation, the lysates were immunoprecipitated with the corresponding antibodies, followed by protein G-Sepharose (GE healthcare, NJ) at 4°C with rotation overnight. After washing three times in lysis buffer, the bound proteins were released by boiling for 5 min in a sample buffer with or without 2-ME. After centrifugation, the supernatants were resolved by sodium dodecyl sulphate polyacrylamide gel electrophoresis (SDS-PAGE) followed a Western blot, as indicated earlier.

Cell adhesion assay

The cell adhesion assay was performed as described by van Kessel (van Kessel et al. 1994), with minor modifications. Briefly, stromal cells were plated in a 96-well plate at 2×10^4 cells/well and were allowed to grow overnight before the adhesion assay. The BM pre-B cells were then labeled by 10 μM of 5-(and 6-) carboxyfluorescein diacetate succinimidyl ester (CFSE) (Molecular Probes, Eugene, OR) for 15 min at 37°C. After labeling, the cells were washed three times and resuspended in RPMI 1640 medium. The labeled cells (5×10^4 cells/well) were added to the stromal cell layer and incubated for 60 min at 37°C. Unbound cells were removed by the addition and removal of prewarmed PBS three times. In each set of experiments, a separate plate containing known numbers of labeled cells was prepared for the determination of a standard curve of fluorescence units per cell. The fluorescence of the adherent cells was quantitated using a fluorescent plate reader (Molecular Device Corp., Sunnyvale, CA) at excitation and emission wavelengths of 485 and 525 nm, respectively. All determinations were in triplicate and the percent adhesion was then calculated as the percentage of bound cells in the plate after washing. Antibodies were added at the same time as the labeled BM pre-B cells. The recombinant mouse VCAM-1/Fc chimera (10 μg/mL PBS with 50 μL/well) (R&D systems, Inc., Minneapolis, MN) was coated on to a 96-well plate at 4°C overnight. After incubation, the plate was washed twice with PBS and then blocked with 1% BSA in PBS for 2 h at 37°C. BM pre-B cells labeled with CFSE were added to the 96-well plate coated VCAM-1/Fc chimera and BSA. After 2 h incubation at 37°C, nonadherent cells were removed by the addition and removal of prewarmed PBS twice. Measurement of fluorescence was done with the fluorescence plate reader as above. Antibodies were added at the same time as the labeled BM cells.

Real-time PCR

Total RNA was prepared from sorted cells using the TRIzol reagent (Invitrogen, Carlsbad, CA), following the protocol recommended by the manufacturer. The real-time PCR analyses were performed by using a Smart Cycler II System (Cephied, Sunnyvale, CA). The cDNA synthesis was performed using SYBR Green Real-time PCR Core Kit (Takara Bio. Inc.) as recommended by manufacturer. Each reaction was performed in a volume of 25 μL, with a final concentration of 1 × SYBR Premix Ex Taq, 200 nM primers, 2 μL of 1:10 dilution of the cDNA, and RNase free water. The thermal cycling conditions for the real-time PCR were 10 s at 95°C to active SYBR Ex Taq, followed by 40 cycles of denaturation for 5 s at 95°C and annealing/extension for 20 s at 60°C. The mean number of cycles for the threshold of fluorescence detection was calculated for each sample, and glyceraldehyde 3-phosphate dehydrogenase (GAPDH) expression was quantified to normalize the amount of cDNA in each sample. The specificity of the amplified products was monitored by its melting curve. The sequences of the real-time PCR primers (Hu et al. 2006) are shown in Table I.

Apoptosis

We used the terminal deoxynucleotidyl transferase-mediated dUTP-biotin nick end labeling (TUNEL) assay performed with a DeadEnd™ Colorimetric TUNEL System (Promega, Madison, WI) as per the manufacturer's recommendations.

Statistical analysis

The results are expressed as mean value ± standard deviation (SD). Statistical analyses were carried out by using the Student's *t*-test. A *P* value of less than 0.05 was considered statistically significant.

Acknowledgements

This work was supported by Core Research for Evolutional Science and Technology (CREST) and the 21st Century Center of Excellence (COE) Program from the Ministry of Education, Science, Culture, Sports, and Technology of Japan, and by the Japan Society for the Promotion of Science (JSPS) Core-to-Core program.

Conflict of interests

None declared.

Abbreviations

α4β1 integrin, very late antigen 4; AOL, *Aspergillus oryzae* lectin; β4GalT-I, β1,4-galactosyltransferase I; BCR, B cell receptor; BM, bone marrow; FUT8, α1,6-fucosyltransferase; GAPDH, glyceraldehyde 3-phosphate dehydrogenase; GnT III, *N*-acetylglucosaminyltransferase III; KD, knockdown; PBS, phosphate-buffered saline; siRNA, short interfering RNA; VCAM-1, vascular cell adhesion molecule 1.

References

Alon R, Kassner PD, et al. 1995.The integrin VLA-4 supports tethering and rolling in flow on VCAM-1. J Cell Biol. 128:1243–1253.

Arroyo AG, Yang JT, et al. 1999. Alpha4 integrins regulate the proliferation/differentiation balance of multilineage hematopoietic progenitors in vivo. Immunity. 11:555–566.

Bany-Laszewicz U, Kaminska J, et al. 2004. The activity of alpha 1,6-fucosyltransferase during human megakaryocytic differentiation. Cell Mol Biol Lett. 9:145–152.

Calderwood DA. 2004. Integrin activation. J Cell Sci. 117:657–666.

Carman CV and Springer TA. 2004. A transmigratory cup in leukocyte diapedesis both through individual vascular endothelial cells and between them. J Cell Biol. 167:377–388.

Carrasco YR and Batista FD. 2006. B-cell activation by membrane-bound antigens is facilitated by the interaction of VLA-4 with VCAM-1. Embo J. 25:889–899.

Delogu A, Schebesta A, et al. 2006. Gene repression by Pax5 in B cells is essential for blood cell homeostasis and is reversed in plasma cells. Immunity. 24:269–281.

Grabovsky V, Feigelson S, et al. 2000. Subsecond induction of alpha4 integrin clustering by immobilized chemokines stimulates leukocyte tethering and rolling on endothelial vascular cell adhesion molecule 1 under flow conditions. J Exp Med. 192:495–506.

Gu J and Taniguchi N. 2004. Regulation of integrin functions by N-glycans. Glycoconj J. 21:9–15.

Guo HB, Lee I, et al. 2002. Aberrant N-glycosylation of beta1 integrin causes reduced alpha5beta1 integrin clustering and stimulates cell migration. Cancer Res. 62:6837–6845.

Hardy RR and Hayakawa K. 2001. B cell development pathways. Annu Rev Immunol. 19:595–621.

Hu H, Wang B, et al. 2006. Foxp1 is an essential transcriptional regulator of B cell development. Nat Immunol. 7:819–826.

Hynes RO. 1992. Integrins: Versatility, modulation, and signaling in cell adhesion. Cell. 69:11–25.

Isaji T, Gu J, et al. 2004. Introduction of bisecting GlcNAc into integrin alpha5beta1 reduces ligand binding and down-regulates cell adhesion and cell migration. J Biol Chem. 279:19747–19754.

Ishida H, Moritani T, et al. 2002. Molecular cloning and overexpression of fleA gene encoding a fucose-specific lectin of Aspergillus oryzae. Biosci Biotechnol Biochem. 66:1002–1008.

Kondo A, Li W, et al. 2006. From glycomics to functional glycomics of sugar chains: Identification of target proteins with functional changes using gene targeting mice and knock down cells of FUT8 as examples. Biochim Biophys Acta. 1764:1881–1889.

Koopman G, Parmentier HK, et al. 1991. Adhesion of human B cells to follicular dendritic cells involves both the lymphocyte function-associated antigen 1/intercellular adhesion molecule 1 and very late antigen 4/vascular cell adhesion molecule 1 pathways. J Exp Med. 173:1297–1304.

Leuker CE, Labow M, et al. 2001. Neonatally induced inactivation of the vascular cell adhesion molecule 1 gene impairs B cell localization and T cell-dependent humoral immune response. J Exp Med. 193:755–768.

Li W, Nakagawa T, et al. 2006. Down-regulation of trypsinogen expression is associated with growth retardation in alpha1,6-fucosyltransferase-deficient mice: attenuation of proteinase-activated receptor 2 activity. Glycobiology. 16:1007–1019.

Lin H and Grosschedl R. 1995. Failure of B-cell differentiation in mice lacking the transcription factor EBF. Nature. 376:263–267.

Luhn K, Wild MK, et al. 2001. The gene defective in leukocyte adhesion deficiency II encodes a putative GDP-fucose transporter. Nat Genet. 28:69–72.

Miyake K, Hasunuma Y, et al. 1992. Requirement for VLA-4 and VLA-5 integrins in lymphoma cells binding to and migration beneath stromal cells in culture. J Cell Biol. 119:653–662.

Miyake K, Medina K, et al. 1991. A VCAM-like adhesion molecule on murine bone marrow stromal cells mediates binding of lymphocyte precursors in culture. J Cell Biol. 114:557–565.

Miyake K, Weissman IL, et al. 1991. Evidence for a role of the integrin VLA-4 in lympho-hemopoiesis. J Exp Med. 173:599–607.

Oz OK, Campbell A, et al. 1989. Reduced cell adhesion to fibronectin and laminin is associated with altered glycosylation of beta 1 integrins in a weakly metastatic glycosylation mutant. Int J Cancer. 44:343–347.

Pelayo R, Welner R, et al. 2005. Lymphoid progenitors and primary routes to becoming cells of the immune system. Curr Opin Immunol. 17:100–107.

Pochec E, Litynska A, et al. 2003. Glycosylation profile of integrin alpha 3 beta 1 changes with melanoma progression. Biochim Biophys Acta. 1643:113–123.

Rossi B, Espeli M, et al. 2006. Clustering of pre-B cell integrins induces galectin-1-dependent pre-B cell receptor relocalization and activation. J Immunol. 177:796–803.

Shinkawa T, Nakamura K, et al. 2003. The absence of fucose but not the presence of galactose or bisecting N-acetylglucosamine of human IgG1 complex-type oligosaccharides shows the critical role of enhancing antibody-dependent cellular cytotoxicity. J Biol Chem. 278:3466–3473.

Singh H, Medina KL, et al. 2005. Contingent gene regulatory networks and B cell fate specification. Proc Natl Acad Sci USA. 102:4949–4953.

Springer TA. 1990. Adhesion receptors of the immune system. Nature. 346:425–434.

Stubbs HJ, Lih JJ, et al. 1996. Influence of core fucosylation on the flexibility of a biantennary N-linked oligosaccharide. Biochemistry. 35:937–947.

Taniguchi N, Miyoshi E, et al. 2006. Decoding sugar functions by identifying target glycoproteins. Curr Opin Struct Biol. 16:561–566.

Urbanek P, Wang ZQ, et al. 1994. Complete block of early B cell differentiation and altered patterning of the posterior midbrain in mice lacking Pax5/BSAP. Cell. 79:901–912.

van Dinther-Janssen AC, Horst E, et al. 1991. The VLA-4/VCAM-1 pathway is involved in lymphocyte adhesion to endothelium in rheumatoid synovium. J Immunol. 147:4207–4210.

van Kessel KP, Park CT, et al. 1994. A fluorescence microassay for the quantitation of integrin-mediated adhesion of neutrophil. J Immunol Methods. 172:25–31.

Vonderheide RH, Tedder TF, et al. 1994. Residues within a conserved amino acid motif of domains 1 and 4 of VCAM-1 are required for binding to VLA-4. J Cell Biol. 125:215–222.

Wadsworth S, Halvorson MJ, et al. 1993. Multiple changes in VLA protein glycosylation, expression, and function occur during mouse T cell ontogeny. J Immunol. 150:847–857.

Wang X, Gu J, et al. 2006. Core fucosylation regulates epidermal growth factor receptor-mediated intracellular signaling. J Biol Chem. 281:2572–2577.

Wang X, Inoue S, et al. 2005. Dysregulation of TGF-beta1 receptor activation leads to abnormal lung development and emphysema-like phenotype in core fucose-deficient mice. Proc Natl Acad Sci USA. 102:15791–15796.

Wilson JR, Williams D, et al. 1976. The control of glycoprotein synthesis: N-acetylglucosamine linkage to a mannose residue as a signal for the attachment of L-fucose to the asparagine-linked N-acetylglucosamine residue of glycopeptide from alpha1-acid glycoprotein. Biochem Biophys Res Commun. 72:909–916.

Yamamoto H, Oviedo A, et al. 2001. Alpha2,6-sialylation of cell-surface N-glycans inhibits glioma formation in vivo. Cancer Res. 61:6822–6829.

Zhao Y, Itoh S, et al. 2006. Deletion of Core Fucosylation on {alpha}3beta1 Integrin Down-regulates Its Functions. J Biol Chem. 281:38343–38350.

Zhuang Y, Soriano P, et al. 1994. The helix-loop-helix gene E2A is required for B cell formation. Cell. 79:875–884.

Int. J. Cancer: **122**, 2301–2309 (2008)

Site-specific analysis of *N*-glycans on haptoglobin in sera of patients with pancreatic cancer: A novel approach for the development of tumor markers

Miyako Nakano[1,2], Tsutomu Nakagawa[1], Toshifumi Ito[3], Takatoshi Kitada[4], Taizo Hijioka[5], Akinori Kasahara[6], Michiko Tajiri[7,8], Yoshinao Wada[7], Naoyuki Taniguchi[2] and Eiji Miyoshi[1,8]*

[1]*Department of Biochemistry, Osaka University Graduate School of Medicine, 2-2 Yamada-oka, Suita, Osaka, Japan*
[2]*Department of Disease Glycomics, Research Institute for Microbial Diseases, Osaka University, 2-1 Yamada-oka, Suita, Osaka, Japan*
[3]*Department of Gastroenterology, Kansai-Rosai Hospital, 3-1-69 Inabaso, Amagasaki, Hyogo, Japan*
[4]*Department of Gastroenterology, Itami City Hospital, 1-100 Koyaike, Itami, Hyogo, Japan*
[5]*Department of Gastroenterology and Hepatology, NHO Osaka-Minami Medical Center, 2-1 Kidohigashimachi, Kawachinagano, Osaka, Japan*
[6]*Department of General Medicine, Osaka University Graduate School of Medicine, 2-2 Yamada-oka, Suita, Osaka, Japan*
[7]*Osaka Medical Center and Research Institute for Maternal and Child Health, 840 Murodo-cho Izumi, Osaka, Japan*
[8]*Japan Science and Technology Agency, 4-1-8 Honcho Kawaguchi, Saitama, Japan*

It was found in our previous studies that the concentration of fucosylated haptoglobin had increased in the sera of patients with pancreatic cancer (PC) compared to those of other types of cancer and normal controls. Haptoglobin, an acute phase protein, has four potential *N*-glycosylation sites, although it remains unknown which site is responsible for the change in fucosylated *N*-glycans. In the present study, site-specific *N*-glycan structures of haptoglobin in sera obtained from patients with PC or chronic pancreatitis (CP) were analyzed using liquid chromatography-electrospray ionization mass spectrometry. Mass spectrometry analyses demonstrated that concentrations of total fucosylated di-, tri- and tetra-branched glycans of haptoglobin increased in the sera of PC patients. Tri-antennary *N*-glycans containing a Lewis X-type fucose markedly increased at the Asn211 site of haptoglobin *N*-glycans. While fucosylated *N*-glycans derived from serum haptoglobin of patients with CP slightly increased, di-fucosylated tetra-antennary *N*-glycans were observed only at this site in PC patients, and were absent in the haptoglobin of normal controls and individuals with CP. Thus, the present study provides evidence that site-specific analyses of *N*-glycans may be useful as novel tumor markers for PC.

Key words: fucosylated haptoglobin; pancreatic cancer; tumor marker; Lewis X; Lewis Y; LC-ESI MS; site-specific analysis

Pancreatic cancer (PC) is one of the leading causes of cancer-related deaths with an overall 5-year survival rate of less than 5%.[1,2] One of the reasons for the poor prognosis is that early diagnosis is quite difficult and risk factors for PC have not yet been identified. Carbohydrate antigen 19-9 (CA19-9) and the carcino embryonic antigen (CEA) are commonly used as markers of PC, but do not allow for early diagnosis.[3] Diagnostic specificity could be increased through a combination of pancreatic tumor markers. To discover novel markers for PC, which have characteristics different from those of CA19-9 or CEA, we used glycomics (see glossary) to identify fucosylated haptoglobin as a potential marker.[4] The addition of glycans to proteins is one of the most important posttranslational modifications carried out, and many studies have shown that changes in glycan structures occur during inflammation and tumorigenesis.[5] Haptoglobin is an acute-phase protein, which is produced in the liver. Since a normal liver expresses low levels of fucosyltransferases and GDP-Fuc (guanosine diphospho fucose, a common donor substrate for fucosyltransferases),[6] most haptoglobin is not fucosylated in healthy individuals.[7,8] Many researchers have reported that fucosylated proteins in serum increase in patients with cancer and/or inflammation.[9–11] Recently, Zhao *et al.*, also reported that several kinds of serum glycoproteins, which were mainly produced in the liver and existed at low levels in serum, increased their fucosylation on *N*-glycans in patients with PC, using glycoprotein microarrays with multi-lectin detection after removing haptoglobin and other major serum proteins.[12] However, it was confirmed in previous study that fucosylated haptoglobin was also produced from certain kinds of PC cells.[4] Therefore, it is important to determine if the increase in fucosylated haptoglobin results directly from PC or is secondary to cancer-induced inflammation of the pancreas. Previously, we found that the appearance rates of fucosylated haptoglobin were higher in patients with PC than those in other types of cancer and normal volunteers (NV).[4] In contrast, it was reported that fucosylated haptoglobin increased in patients with other types of cancer, such as ovary cancer,[13] hepatocellular carcinoma[14] and lung cancer[15] that had progressed to an advanced stage. To gain insight into the mechanism and location of fucosylation up-regulation, more detailed analyses of haptoglobin *N*-glycans are required.

Human haptoglobin is comprised of 406 amino acid residues,[16,17] which consists of a signal peptide (Met1 to Ala18), one α chain (Val19 to Gln160) and one β chain (Ile162 to Asn406). The haptoglobin β chain contains four potential *N*-glycosylation sites (see supplemental Fig. 1): Asn184 (site 1), Asn207 (site 2), Asn211 (site 3) and Asn241 (site 4).[18,19] In the present study, PA-labeled haptoglobin *N*-glycans from patients with chronic pancreatitis (CP) and PC were analyzed using normal-phase HPLC (NP-HPLC) to measure the amount of fucosylated *N*-glycans and to identify the type of fucosylated *N*-glycans (*i.e.*, the linkage position of Fuc). Furthermore, precise analyses of site-specific *N*-glycan structures of haptoglobin were carried out using liquid chromatography-electrospray ionization mass spectrometry (LC-ESI MS, see glossary) to identify fucosylated *N*-glycans unique to PC.

Material and methods

Lysylendopeptidase was obtained from Wako Pure Chemical Industries Ltd. (Osaka, Japan). Sequencing-grade modified trypsin was purchased from Promega (Madison, WI). Polyclonal rabbit

This article contains supplementary material available via the Internet at http://www.interscience.wiley.com/jpages/0020-7136/suppmat.

Grant sponsors: the 21st Century COE program Osaka University, Japan Science and Technology Agency (JST).

***Correspondence to:** Department of Molecular Biochemistry & Clinical Investigation, Osaka University Graduate School of Medicine, Division of Health Science, 1-7 Yamada-oka, Suita, 565-0871, Japan.
Fax +81-6-6879-2590. E-mail: emiyoshi@sahs.med.osaka-u.ac.jp

Received 23 July 2007; Accepted after revision 20 November 2007
DOI 10.1002/ijc.23364
Published online 23 January 2008 in Wiley InterScience (www.interscience.wiley.com).

anti-human haptoglobin antibody was obtained from DakoCytomation (Glostrup, Denmark). Endoprotease Glu-C and Peptide-N^4-(acetyl-β-D-glucosaminyl) asparagine amidase (PNGase F; E.C. 3.5.1.52, recombinant) were purchased from Roche Molecular Biochemicals (Tokyo, Japan). Aleuria aurantia lectin (AAL) conjugated with biotin was purchased from Honen Corp. (Tokyo, Japan). Horseradish peroxidase-conjugated streptavidin was obtained from Pierce, (Rockford, IL). Alpha 1-3/4 fucosidase and PA-labeled glycan standards for HPLC analysis were obtained from Takara Bio Inc (Shiga, Japan). Beta 1-4 galactosidase derived from *S. pneumoniae* was obtained from PROenzyme Co. (San Leandro, CA). Other reagents were either of the highest quality or were LC/MS grade, commercially available.

Serum samples

Serum samples from patients with PC (PC 1–5; $n = 5$, male 2, female 3, mean age 65 years) and CP (CP 1–5; $n = 5$, male 3, female 2, mean age 66 years) were obtained from Osaka University-related Hospitals. Serum samples from NV (NV 1-8; $n = 8$, male 5, female 3, mean age 46 years) were obtained in our laboratory with the participants' informed consent. NV 1-5 and NV 6–8 sera samples were respectively obtained from NV 26–38 and 63–75 years of age. All serum samples were stored at −80°C until used. The present project was approved by the ethics committees of the participating hospitals and Osaka University.

For a clear understanding, all procedures we performed in the present study are described in the workflow (Supplemental Fig. 2).

Purification and SDS-PAGE analysis of haptoglobin from human sera

The sera of patients with PC (100 μL), CP (100 μL) and of NV (300 μL) were filtered using a 0.45-μm filter (Minisart RC 15, Sartorius, Goettingen, Germany) and then diluted with buffer A (50 mM sodium phosphate buffer (pH 7.4), 0.5 M NaCl, 0.02% NaN_3) to a final volume of 7 mL. The diluted serum samples were circulated 5 times on an anti-haptoglobin affinity column, which was coupled with 300 μL of anti-human haptoglobin, at room temperature, according to the standard protocols of HiTrap NHS-activated HP (1 mL) (GE Healthcare, Uppsala, Sweden), using a peristaltic pump. After washing the column with 15 mL of buffer A, the haptoglobin bound to the column was eluted with 5 mL of elution buffer (100 mM Glycine, 0.5 M NaCl, pH 3.0). The eluate was immediately neutralized with 100 μL of 2 M Tris-HCl (pH 8.0). The neutralized eluate containing haptoglobin was passed through a PD-10 column (GE Healthcare) equilibrated with water to remove glycine, NaCl and Tris-HCl. The aqueous solution containing haptoglobin was evaporated to dryness. The residue was dissolved in 100 μL of water (sample solution A), and a portion (5 μL) was used for SDS-PAGE analysis to determine the haptoglobin yield. The solution (7 mL) containing proteins, which were not adsorbed to the anti-human haptoglobin column, were mixed with the washed column solution (15 mL), and the mixture was evaporated to dryness. The residue, which contained the pass-through fraction, was dissolved in 1 mL of water. The 10-fold diluted serum (5 μL), the pass-through fraction (5 μL) and the eluted fraction (sample solution A, 5 μL) were all subjected to SDS-PAGE (10% polyacrylamide) under reduced conditions and then stained with CBB.

LC-ESI MS identification of proteins purified using an anti-human haptoglobin column

The eluted solutions from the anti-human haptoglobin column (sample solution A, 80 μL) were evaporated to dryness, and 500 μL of a reducing solution containing 250 mM Tris-HCl (pH 8.5), 6 M guanidine hydrochloride, 2 mM EDTA and dithiothreitol (10 mg) were added to the residue. The mixture was incubated at 50°C for 1 hr to reduce Cys residues. After adding iodoacetamide (20 mg) to the mixture, the reaction was allowed to proceed for 30 min at room temperature in the dark. The reaction mixture was passed through a Nap-5 column (GE Healthcare) equilibrated with 0.05 N HCl to remove salts from the reducing solution and excess iodoacetamide. The eluate containing *S*-carbamidomethylated haptoglobin (1 mL, in 0.05 N HCl) was immediately neutralized with 100 μL of 1 M Tris-HCl (pH 9.0). The neutralized solution was mixed with 20 μL of 50 mM Tris-HCl (pH 8.5) containing an enzyme mixture of lysylendopeptidase (2 μg) and trypsin (2 μg) and incubated for 16 hr at 37°C.[20] After boiling, the solution was evaporated to dryness. The residue was dissolved in 100 μL of water (sample solution B). The tryptic peptide mixture (sample solution B, 10 μL) was separated using an ODS column (Develosil 300ODS-HG-5, 150 × 1.0 mm i.d., Nomura Chemical, Aichi, Japan) under the following gradient conditions. The mobile phases were: (A) 0.1% TFA and (B) 0.1% TFA/80% acetonitrile. The gradient elution was performed at 10–60% B for 80 min with a flow rate of 50 μL/min using an Agilent 1100 series HPLC system (Agilent Technologies, Santa Clara, CA). The eluate was continuously introduced into an electrospray ionization (ESI) source (Esquire HCT, Bruker Daltonics GmbsH, Bremen, Germany). The proteins were identified using the NCBInr database with the MASCOT (Matrix Science, Boston, MA) database-searching algorithm.

Lectin blot analysis

Purified haptoglobin was subjected to SDS-PAGE (10% polyacrylamide) under reduced conditions. The gels were visualized by CBB staining, and the bands on the gels were quantified using an Image Reader LAS-3000 mini/Multi Gauge ver 2.2 (Fuji Photo Film, Tokyo, Japan). On the basis of the quantification results, equivalent amounts of purified haptoglobin were applied in duplicate to two SDS-PAGE gels. The proteins on one gel were stained with CBB, while those on the other gel were transferred to a PVDF membrane under semi-dry conditions by means of a Trans-blot (Bio-Rad, Hercules, CA). All AAL blot procedures have previously been described in detail.[4] Briefly, after blocking by incubation with 2% BSA, the membrane was incubated with AAL conjugated with biotin followed by incubation with horseradish peroxidase-conjugated streptavidin. The chemiluminescence method with the ECL-Plus kit (GE Healthcare) was employed to detect the peroxidase activity. The samples were visualized using a LAS-3000 mini.

NP-HPLC analysis of PA-labeled N-glycans

The aqueous solution containing tryptic peptides treated with iodoacetamide (sample solution B, 10 μL) was mixed with 2 M acetic acid (100 μL), and the mixture was incubated at 80°C for 2 hr to remove sialic acids. After evaporating to dryness, the residue was digested with PNGase F (0.1 U in 50 μL of 50 mM NH_4HCO_3) to release the *N*-glycans. The released *N*-glycans were applied to a GlycoTAG apparatus (Takara Bio Inc) for derivatization with PA.[21] Furthermore, a portion of PA-labeled *N*-glycans was digested with α1-3/4 fucosidase[22] followed by digestion with β1-4 galactosidase. The PA-labeled *N*-glycans were subjected to NP-HPLC analysis. Eight types of commercially available PA-labeled *N*-glycans, shown in Figure 2*b*, were analyzed (10 pmol each) as standards. HPLC was performed with a Waters Alliance System equipped with a Waters 2475 fluorescence detector. Separation was done at 50°C using a polymer-based Asahi Shodex NH2P-50 4E column (Showa Denko, Tokyo, Japan; 4 × 250 mm) with a linear gradient formed by 2% acetic acid in acetonitrile (solvent A) and 5% acetic acid in water containing 3% triethylamine (solvent B). The column was initially equilibrated and eluted with 30% solvent B for 2 min, at which point the concentration of solvent B was increased to 50% over 60 min. The flow rate was 1.0 mL/min throughout the analysis. Detection was performed by fluorometry at $\lambda_{ex} = 320$ nm and $\lambda_{em} = 400$ nm.

LC-ESI MS analysis of haptoglobin sialo-glycopeptides at sites 1 and 4

Analyses of haptoglobin sialo-glycopeptides containing *N*-glycans at binding sites 1 and 4 simultaneously were performed with identification of haptoglobin using LC-ESI MS (see the section

"LC-ESI MS identification of proteins purified using an anti-human haptoglobin column").

Preparation of asialo-glycopeptide and digestion with endoprotease Glu-C

Enrichment of glycopeptides from tryptic digests was carried out using affinity separation by partitioning with Sepharose CL4B, according to the method described by Wada *et al.*[23] Briefly, water (150 μL) was added to the tryptic digests (sample solution B, 50 μL), and the solution was mixed with 1 mL of an organic solvent of 1-butanol/ethanol (4:1, v/v). The mixture was added to a 1.5-mL polypropylene tube containing 100 μL packed volume of Sepharose CL4B equilibrated with 1-butanol/ethanol/H_2O (4:1:1, v/v). After gentle shaking for 30 min, the gel was washed three times with the same organic solvent (1 mL). The gel was then incubated with an aqueous solvent, ethanol/H_2O (1:1, v/v), for 10 min, and the liquid-phase was evaporated to dryness. The residue was dissolved in 2 M acetic acid (100 μL) to remove sialic acids. After incubation for 2 hr at 80°C, the solution was evaporated to dryness. The residue was dissolved in 40 μL of water, and a portion (10 μL) was mixed with endoprotease Glu-C (1 μg in 30 μL of 50 mM NH_4HCO_3). The mixture was incubated for 16 hr at 37°C, and then boiled (sample solution C).

LC-ESI MS analysis of haptoglobin asialo-glycopeptides at sites 2 and 3

The solution containing asialo-glycopeptides digested with trypsin and endoprotease Glu-C (sample solution C, 10 μL) was subjected to LC-ESI MS analysis. The asialo-glycopeptides were separated using an ODS column (Develosil 300ODS-HG-5, 150 × 1.0 mm i.d., Nomura Chemical, Aichi, Japan) under the following gradient conditions. The mobile phases were: (A) 0.08% formic acid and (B) 0.15% formic acid/80% acetonitrile. The column was eluted with solvent A for 5 min, at which point the concentration of solvent B was increased to 50% over 75 min at a flow rate of 50 μL/min. The eluate was continuously introduced into an ESI source (Esquire HCT).

Relative abundance of N-glycan structures at each haptoglobin site

The relative abundance of each glycoform at sites 1–4 was calculated based on the signal intensities of the corresponding glycopeptides obtained by LC-ESI MS analysis.[24] Briefly, total signal intensities of glycopeptides detected as sialylated-*N*-glycopeptides were set to 100% for each site of each sample, and the average ratio for each sialo-glycopeptide glycoform was calculated for young NV (under 40), old NV (over 60), CP and PC samples. When the ratio was expressed for asialoforms, the average ratios of sialo-glycopeptides thus obtained were converted to those of asialo-glycopeptides based on the predicted structures of asialo-glycoforms, while the value obtained by direct calculation was used for the desialylated samples (sites 2 and 3).

Results

Purification of human haptoglobin from sera and AAL blot analysis

Haptoglobin was purified from the sera of five patients with PC, CP and the sera of eight NV. A representative result of purified haptoglobin from a patient with PC (sample PC1) is shown in Figure 1*a*. A 40-kDa band, a haptoglobin β-chain, was detected as the major band without contaminant bands in the eluted fraction, demonstrating that haptoglobin was obtained with high-purity. A portion of the eluted fraction was digested with a combination of trypsin and lysylendopeptidase,[19] and the digests were analyzed by LC-ESI MS to confirm that the 40-kDa protein was haptoglobin. The peptides detected by ESI MS were confirmed to be derived from haptoglobin with high probability scores by peptide mass fingerprinting against the NCBInr database (data not shown).

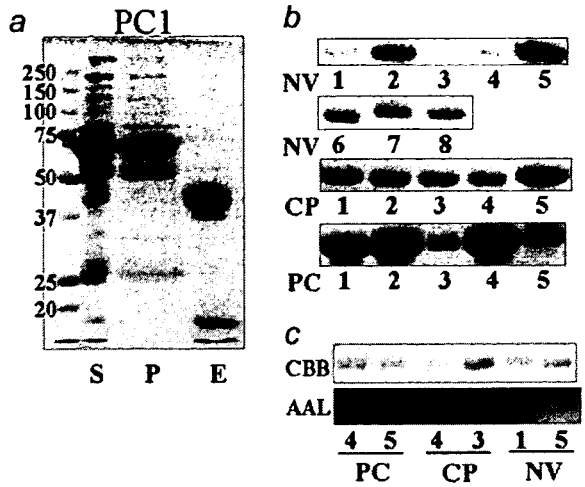

FIGURE 1 – Purification of haptoglobin using an anti-haptoglobin affinity column and AAL blot analysis. (*a* and *b*), all gels were stained with CBB after SDS-PAGE analysis (10% polyacrylamide). (*a*) SDS-PAGE analysis of serum (S), pass through fraction (P), and eluted fraction (E) from sera of patients with pancreatic cancer (PC1). (*b*) purified haptogoboin from sera of patients with pancreatic cancer (PC), chronic pancreatitis (CP), and sera of normal volunteers (NV). The volume of NV applied was 3-fold greater than the sample volumes of CP and PC. (*c*) equal amounts of purified haptoglobin from PC, CP, and NV were electrophoresed, followed by CBB staining and AAL blot analysis (2 samples each).

To evaluate the levels of haptoglobin in the serum of patients with PC and CP compared to those of NV, the samples of purified haptoglobin were electrophoresed on 10% polyacrylamide gels, followed by staining with CBB (Fig. 1*b*). Haptoglobin slightly increased in all 5 patients with CP; furthermore, the 3 patients with PC also had elevated haptoglobin levels. This result may be attributed to the fact that haptoglobin is an acute-phase protein.

To determine the variation in fucosylated glycans, AAL blot analysis of purified haptoglobin was performed. AAL interacts with α1-2 Fuc, α1-3/4 Fuc and α1-6 Fuc on glycans.[25,26] Equal amounts of purified haptoglobin were subjected to AAL blot analysis. As shown in Figure 1*c*, haptoglobin from patients with PC exhibited strong AAL binding. This result indicated that haptoglobin *N*-glycan structures changed in patients with PC-especially in terms of the number of Fuc residues.

NP-HPLC analysis of PA-labeled N-glycans derived from haptoglobin

Sialic acids were removed from *N*-glycan on tryptic peptides using acidic treatment. The asialo *N*-glycans were released with PNGaseF and were derivatized with PA. PA-labeled *N*-glycans were analyzed by NP-HPLC using an amino column. Eight commercially available PA-labeled *N*-glycans, shown in Figure 2*b*, were used as standards (Fig. 2*a*). More detailed structures of the standard *N*-glycans are shown in supplemental Figure 3*a*. The chromatograms for NV5, CP3 and PC4 are shown in Figure 2*a*. Tri-antennary *N*-glycan containing core Fuc (*i.e.*, α1-6 Fuc, peak 4) was not detected in any of the samples. Bi-antennary *N*-glycan (peak 1*) was the most abundant peak in all samples. Peaks 5* and 8* increased in the PC4 sample compared to the NV5 and CP3 samples. Although the composition of *N*-glycan in peak 5* was predicted to be tri-antennary *N*-glycan containing a Lewis X-type Fuc (*i.e.*, α1-3 Fuc), there were at least 4 possible structures (Lewis X, Lewis A, H1 and H2 in Fig. 2*c*) that were eluted at the same time. These 4 types of *N*-glycans have the same molecular weight and consist of the same numbers of the same kinds of monosaccharides, but the linkage position and linkage type of the Gal